

A NONISOTHERMAL THERMODYNAMICAL MODEL OF LIQUID-VAPOR INTERACTION WITH METASTABILITY

HALA GHAZI, FRANÇOIS JAMES, AND HÉLÈNE MATHIS

ABSTRACT. The paper concerns the construction of a compressible liquid-vapor relaxation model which is able to capture the metastable states of the non isothermal van der Waals model as well as saturation states. Starting from the Gibbs formalism, we propose a dynamical system which complies with the second law of thermodynamics. Numerical simulations illustrate the expected behaviour of metastable states: an initial metastable condition submitted to a certain perturbation may stay in the metastable state or reaches a saturation state. The dynamical system is then coupled to the dynamics of the compressible fluid using an Euler set of equations supplemented by convection equations on the fractions of volume, mass and energy of one of the phases.

Key-words. Thermodynamics of phase transition, metastable states, van der Waals EoS, dynamical systems, homogeneous relaxation model, numerical simulations.

MSC. 2010 80A10, 80A15, 37N10.

CONTENTS

1. Introduction	1
2. Thermodynamic assumptions and the van der Waals EoS	4
2.1. Description of a single fluid	4
2.2. The van der Waals Equation of State	5
3. Thermodynamics of equilibria for a multicomponent system	9
3.1. The Gibbs phase rule	10
3.2. Maxima of the constrained optimization problem	11
4. Dynamical system and attraction bassins	13
4.1. Equilibria and attractivity	14
4.2. Numerical illustrations	17
5. An homogeneous relaxation model	24
5.1. Properties of the homogeneous relaxation model	26
5.2. Numerical illustrations	30
6. Conclusion	31
References	33

1. INTRODUCTION

Metastable two-phase flows are involved in many industrial applications, for instance in scenarii of safety accidents in pressurized water reactors. They can also

appear in everyday life. Warming water in a microwave with the maximum power may make the liquid water being metastable: its temperature increases above the saturation temperature; the water is then called superheated. The metastability corresponds then to a delay in vaporization. Even a small perturbation of the metastable water may lead to the brutal appearance of a vaporization wave. In [4] an analogous phenomenon is highlighted. Liquid water can be brought to a superheated state by means of a very rapid depressurization. The depressurization is stopped suddenly by an explosive nucleation causing, in its turn, an increase of the pressure.

As pointed out in [7], such compressible two-phase flows are characterized by three main difficulties. The first two difficulties are linked to the dynamics of the fluid, namely the compressibility of both phases and the presence of the moving interface between them. The third difficulty lies in the modelling of the thermodynamical exchanges which occur at the interface. The references [26] and [28] focus on the two first difficulties and propose models coming from the Bear-Nunziato model for compressible two-phase flows. The models are either 6 or 5 equations models, possibly including pressure and velocity interfacial terms. Each phase possesses its own convex Equation of State (EoS), namely a stiffened gas law (or a Mie-Grüneisen generalization). Relaxation towards thermodynamical equilibrium is assumed to be infinitely fast, so that metastable states appear far from the vaporization fronts. In [7, 8] and [9], the authors improve this approach by using the realistic tabulated law IAPWS-IF97 EoS coupled with cubic interpolation and accurate HLLC-type numerical scheme. They compare different models of a same hierarchy. Starting from a single-velocity six equations model with full disequilibrium, they consider an homogeneous equilibrium model where the liquid and the vapor are at thermodynamical equilibrium (meaning stable) and a homogeneous relaxation model in which the liquid is assumed to be metastable and the vapor is at saturation. Again emphasis is given to the two first difficulties of compressible two-phase flows, the question of metastability being addressed solely in the choice of the complex EoS.

In the present paper, we focus on the third difficulty, namely the modelling of thermodynamical transfers and the appearance of metastable states. As the dynamics of the flow is concerned, we adopt the strategy proposed in [7, 8] and consider the homogeneous relaxation model given in [16] and [20]. We assume that the two phases evolve with the same velocity and consider the mass, momentum and energy conservation equation of the flow. The specificity is to assume that the two phases follow the same non-convex EoS, namely a reduced form of the van der Waals equation. Because the model involves a mixture pressure based on this cubic equation, the convective system is not strictly hyperbolic, notably in the van der Waals spinodal zone. To get rid of this problem, the pressure is relaxed and depends on additional quantities, which are the fractions of volume, mass and energy of one of the phases. These fractions obey to convective equations with relaxation terms towards the thermodynamic equilibrium. The core of the paper is the proper definition of these relaxation terms. To do so, we extend the method we proposed in [22] in the isothermal case and provide a characterization of thermodynamic equilibria which are either saturation states, stable and metastable states.

In a first section, we recall some basic facts of thermodynamics in the extensive and intensive form [5], notably the notion of entropy. We focus on the van der Waals model, which is well-known to depict stable and metastable states but is classically used with a convexification correction to properly depict saturation. It turns out that the representation of metastable states of the van der Waals model is done in the volume-pressure plane, although the equations of motion require to manipulate phase diagram and EoS defined in the volume-energy plane. A large part of Section 2.2 then concerns the representation of stable, metastable and spinodal zone in the volume-energy plane.

In Section 3 we investigate the thermodynamic stability of a system described by the non convex EoS of van der Waals in its reduced form. As suggested in [5, chap. 8], introducing heterogeneity in a system is the hallmark of phase transition. Hence, in order to introduce heterogeneity in the system, we decompose it in an arbitrary number of subsystems depicted by the same nonconvex EoS. The second principle of thermodynamics leads to a constrained maximization problem on the mixture entropy. It turns out that the number of subsystems is limited to two, in accordance with the Gibbs phase rule. Then the study of the optimization problem leads to two possible kinds of maximizers, either saturation states or states corresponding to the identification of the two phases. In the latter case, there is no distinction between the two phases and all the states belonging to the van der Waals EoS are possible maximizers, including the non-admissible (physically unstable) states of the spinodal zone. On the other hand, the saturation states correspond to the coexistence of the two phases at saturation, with equality of the pressures, temperatures and chemical potentials of the two phases, corresponding to the convexification of the EoS.

Section 4 provides a dynamical description of the thermodynamic equilibrium and of its two kind of equilibrium states. Following the approach developed in [22] and [14] in the isothermal case, we introduce a dynamical system whose long-time equilibria coincide with the maxima of the above optimization problem, under a mixture entropy growth criterion. We focus in this paper on a dynamical system on the fractions of volume, mass and energy of the phase 1. The system is designed to recover the above two possible equilibria: either saturation states or states corresponding to the identification of the two phases. In the latter case, the equilibrium is characterized by the equality of all the fractions which converge asymptotically to some value belonging to $]0, 1[$. Hence, as the two phases identify, the fractions are not equal to 0 or 1, in contrast with the Baer-Nunziato type two-phase models [1]. This is one fundamental feature of the dynamical model we propose. Another property stands in the attractivity of the equilibria and their attraction basins. If the energy-volume state of the mixture belongs to the spinodal zone, then the corresponding equilibrium is a saturation state, whatever the initial conditions of the dynamical system are. Thus the dynamical system gets rid of unstable states of the spinodal zone by construction. On the other hand, if the mixture state belongs to a metastable zone, there are two possible equilibria depending on the perturbation: either the identification of the two phases to the mixture metastable state or a saturation state. This interesting property was already highlighted in [22, 14] and is extended here to the non-isothermal case. Numerical simulations illustrate the attraction of each equilibria and typical trajectories of the dynamical system in the volume-energy plane, volume-pressure plane and in the fractions domain.

Finally Section 5 addresses the coupling between the thermodynamics and the compressible dynamics of the two-phase flows we are interested in. Following the approach in [16, 20, 7], we consider that the fluid is homogeneous in the sense that the two phases evolve with the same velocity. Then the model is based on the conservation equations of total mass, momentum and energy. To close the system, it is endowed with a complex equation of state depending on the fractions of volume, mass and energy of one of the phases. To ensure the return to the thermodynamic equilibrium, the evolution equations of the fractions admit relaxation source terms derived from the dynamical system studied in Section 4. Because the mixture pressure involves the van der Waals EoS, the hyperbolicity is non strict. However it has been proved in [22] that the domains of hyperbolicity of the complete model strongly depend on the attraction basins of the dynamical system. In order to illustrate the dynamical behaviour of the model, we provide a numerical scheme based on a fraction step approach: the convective part is approximated by an explicit HLLC solver while the source terms is integrated by a RK4 method.

2. THERMODYNAMIC ASSUMPTIONS AND THE VAN DER WAALS EOS

2.1. Description of a single fluid. We consider a monocomponent fluid of mass $M \geq 0$, occupying a volume $V \geq 0$ with internal energy $E \geq 0$. Following the Gibbs formalism [15, 5], we introduce the extensive entropy S of the fluid as a function of its mass M , volume V and energy E :

$$(1) \quad S : (M, V, E) \mapsto S(M, V, E).$$

All the above quantities are said extensive, in the sense that if the system is doubled, then its mass, volume, energy and entropy are doubled as well. Any extensive quantity is said positively homogeneous of degree 1 (PH1) and satisfies

$$(2) \quad \forall \lambda > 0, \quad S(\lambda M, \lambda V, \lambda E) = \lambda S(M, V, E).$$

We assume that the entropy function S belongs to $C^2(\mathbb{R}^+ \times \mathbb{R}^+ \times \mathbb{R}^+)$. It allows to introduce intensive quantities, that are positively homogeneous functions of degree 0 (PH0), corresponding to derivatives of extensive functions. From the gradient vector ∇S of the entropy S , we commonly define the pression p , the temperature T and the chemical potential μ by

$$(3) \quad \frac{1}{T} = \frac{\partial S}{\partial E}(M, V, E), \quad \frac{p}{T} = \frac{\partial S}{\partial V}(M, V, E), \quad \frac{\mu}{T} = -\frac{\partial S}{\partial M}(M, V, E),$$

leading to the fundamental thermodynamics extensive Gibbs relation

$$(4) \quad dS = -\frac{\mu}{T}dM + \frac{p}{T}dV + \frac{1}{T}dE.$$

Standard thermodynamics requires that

$$(5) \quad T = \left(\frac{\partial S}{\partial E} \right)^{-1} > 0.$$

Since the entropy S is a PH1 function, it verifies the Euler relation

$$(6) \quad S(M, V, E) = \nabla S(M, V, E) \cdot \begin{pmatrix} M \\ V \\ E \end{pmatrix},$$

which, combined with the definitions (3), gives

$$(7) \quad S(M, V, E) = -\frac{\mu M}{T} + \frac{pV}{T} + \frac{E}{T}.$$

Introducing the specific volume $\tau = V/M$ and the specific internal energy $e = E/M$, and using the homogeneity of the extensive entropy function, one can define the specific entropy s

$$(8) \quad s(\tau, e) = S\left(1, \frac{V}{M}, \frac{E}{M}\right) = \frac{1}{M}S(M, V, E).$$

We keep the same notations to denote the pressure and the temperature expressed as functions of the specific volume and energy

$$(9) \quad \frac{1}{T} = \frac{\partial s}{\partial e}(\tau, e), \quad \frac{p}{T} = \frac{\partial s}{\partial \tau}(\tau, e).$$

The fundamental thermodynamics relation in its intensive form reads as follow

$$(10) \quad Tds = de + pd\tau.$$

and the intensive counterpart of relation (7) is

$$(11) \quad Ts = -\mu + p\tau + e.$$

2.2. The van der Waals Equation of State. In this work we focus on a non necessarily concave nor convex entropy function s . A common exemple is the van der Waals Equation of State (EoS), which entropy reads

$$(12) \quad s(\tau, e) = C_v \ln\left(\frac{a}{\tau} + e\right) + R \ln(\tau - b) + s_0,$$

where R is the universal constant of gas, $C_v > 0$ the calorific constant at constant volume, s_0 is the entropy of reference, and a and b are the two nonnegative parameters [5, 23].

The entropy is well defined for $(\tau, e) \in (\mathbb{R}^+)^2$ such that

$$(13) \quad \tau > b, \quad \frac{a}{\tau} + e > 0.$$

The corresponding definition domain of s is denoted D_s :

$$(14) \quad D_s := \left\{ (\tau, e) \in (\mathbb{R}^+)^2; \tau > b \text{ and } \frac{a}{\tau} + e > 0 \right\}.$$

According to relations (9), the van der Waals temperature and pressure read

$$(15) \quad T(\tau, e) = \frac{1}{C_v} \left(e + \frac{a}{\tau} \right),$$

$$(16) \quad p(\tau, e) = \frac{R}{C_v(\tau - b)} \left(e + \frac{a}{\tau} \right) - \frac{a}{\tau^2} = \frac{RT(\tau, e)}{\tau - b} - \frac{a}{\tau^2}.$$

The van der Waals entropy is neither concave nor convex. Indeed the coefficients of its Hessian matrix $H_s(\tau, e)$ are given by

$$(17) \quad \begin{cases} \frac{\partial^2 s}{\partial \tau^2}(\tau, e) = \frac{1}{T(\tau, e)} \left(\frac{2a}{\tau^3} - \frac{a}{\tau^2} \frac{R}{C_v(\tau - b)} - \frac{RT(\tau, e)}{(\tau - b)^2} \right) + \frac{a}{C_v} \frac{p(\tau, e)}{\tau^2 T^2(\tau, e)}, \\ \frac{\partial^2 s}{\partial e^2}(\tau, e) = -\frac{C_v}{T^2(\tau, e)}, \\ \frac{\partial^2 s}{\partial \tau \partial e}(\tau, e) = \frac{C_v}{T^2(\tau, e)} \frac{a}{\tau^2}. \end{cases}$$

Since the temperature T is positive on D_s , one has

$$(18) \quad \frac{\partial^2 s}{\partial e^2} < 0.$$

However the entropy function s is not globally concave and its domain of concavity restricts to the set where the determinant of H_s is positive, that is

$$(19) \quad D_c := \left\{ (\tau, e) \in D_s; \frac{\partial^2 s}{\partial \tau^2} \frac{\partial^2 s}{\partial e^2} - \left(\frac{\partial^2 s}{\partial e \partial \tau} \right)^2 > 0 \right\}.$$

The non-concavity property of the van der Waals entropy makes it an appropriate toy-model to represent liquid-vapor phase transition [5, chap.9]. States belonging to the concavity region of the entropy refer to stable and metastable liquid and vapor states. In contrast states belonging to the non-concavity region are non-admissible states. The purpose of this section is to precise the geometrical loci of these states and provide representations of the phase diagrams of the van der Waals EoS in both the (τ, p) and the (τ, e) planes.

In all the representations given in the sequel, we use a reduced form of the EoS, as the one proposed in [11], with the parameters

$$(20) \quad a = 1, \quad b = 0.5, \quad R = 0.5, \quad C_v = 3, \quad s_0 = 0.$$

Usually the metastable zones of the van der Waals EoS are defined and observable in the (τ, p) plane at constant temperature. This implies to manipulate the entropy and the pressure as functions of the volume τ and the temperature T . Adapting relations (15), (16) and (12) leads to

$$(21) \quad \begin{aligned} s(\tau, T) &= C_v \ln(C_v T) + R \ln(\tau - b) + s_0, \\ p(\tau, T) &= \frac{RT}{\tau - b} - \frac{a}{\tau^2}. \end{aligned}$$

We represent in Figure 1 the isothermal curves $(\tau, p(\tau, T))$ (black lines) in the (τ, p) plane for fixed temperatures T . There exists a unique critical temperature T_c for which the pressure admits a unique inflection point $(\tau_c, p(\tau_c, T_c))$, called the critical point. For the reduced van der Waals law, $T_c = 1$. For supercritical temperature $T > T_c$, the pressure is a strictly decreasing function of the specific volume. Below the critical isothermal curve, for $T < T_c$, the pressure is an increasing function of the volume between the minimum $(\tau_-, p(\tau_-, T))$ and the maximum $(\tau_+, p(\tau_+, T))$. This increasing branch refers to non physically admissible states. The critical isothermal curve is plotted in green in Figure 1. The set of minima and maxima is plotted in blue in Figure 1 and delimits the spinodal zone. Actually the spinodal zone in the (τ, p) plane corresponds to the zone $D_s \setminus D_c$ in the plane (τ, e) where the entropy function is not concave.

At a given temperature $T < T_c$, it is classical to replace the non admissible increasing branch of the pressure by a specific isobaric line satisfying the Maxwell equal area rule. Such a construction defines two volumes τ_1^* and τ_2^* , for each temperature $T < T_c$, such that $p(\tau_1^*, T) = p(\tau_2^*, T)$. Their set, represented in red in Figure 1, is called the saturation dome. The states belonging to decreasing branches of isothermal curves, below the saturation dome (in red) and above the spinodal zone (in blue) are called metastable states.

The purpose of this section is to provide a representation of the saturation dome, spinodal and metastable zones in the (τ, e) plane. We represent in Figure 2 the

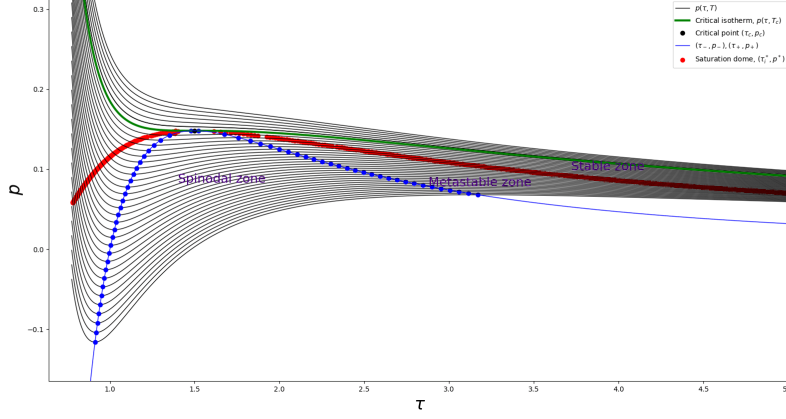


FIGURE 1. Isothermal curves of the van der Waals EoS in the (τ, p) plane. Isothermal curves $p(\tau, T)$ are plotted in black. The isothermal curve at critical temperature $T = T_c$ is plotted in green. Below the critical isothermal curve, the pressure is not monotone with respect to the specific volume and increases in the spinodal zone of non admissible states. This zone is delimited by the blue curve representing the set of minima $(\tau_-, p(\tau_-, T))$ and maxima $(\tau_+, p(\tau_+, T))$ of the pressure for each temperature $T < T_c$. The Maxwell equal area rule construction allows to replace the non physically admissible increasing branch of an isothermal curve by computing two volumes τ_1^* and τ_2^* at each temperature $T < T_c$, such that $p(\tau_1^*, T) = p(\tau_2^*, T)$. The set of these volumes is represented in red in the graph and corresponds to the saturation dome. The states belonging to decreasing branches of isothermal curves, below the saturation dome (in red) and above the spinodal zone (in blue), are called metastable states.

isothermal curves in the (τ, e) plane. The spinodal zone corresponds to the domain where the concavity of the entropy function $(\tau, e) \mapsto s(\tau, e)$ changes. According to the definition (17) of the Hessian matrix $H_s(\tau, e)$ of the entropy s , this domain is delimited by the set of states $(\tau, e) \in D_s$ such that

$$(22) \quad \det(H_s)(\tau, e) = 0.$$

Solving (22) allows to define the spinodal zone $Z_{\text{Spinodal}} \subset D_s$

$$(23) \quad Z_{\text{Spinodal}} := \{(\tau, e) \in D_s; e < g(\tau)\},$$

where

$$(24) \quad g(\tau) = \frac{2aC_v(\tau - b)^2}{R\tau^3} - \frac{a}{\tau}.$$

The critical isothermal curve (green curve) admits a unique intersection point with the graph of g which turns to be the critical point $(\tau_c, e_c = g(\tau_c))$. The Maxwell construction, which is usually defined in the (τ, p) -plane, admits its counterpart

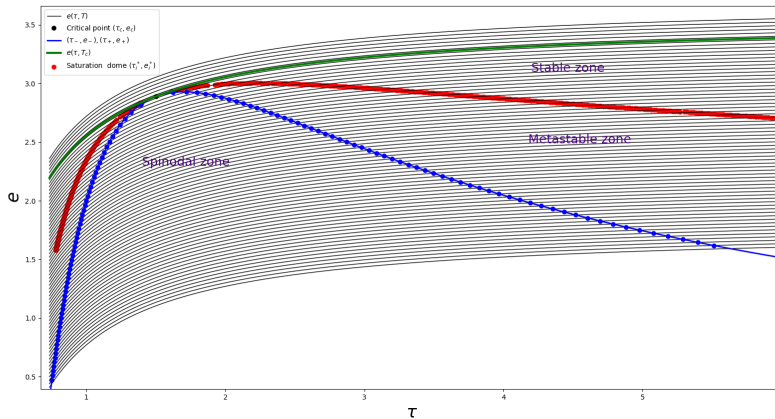


FIGURE 2. Isothermal curves of the van der Waals EoS in the (τ, e) -plane. The black lines correspond to isothermal curves $e(\tau, T)$. The isothermal curve at the critical temperature $T = T_c$ is plotted in green. States belonging to the zone above the critical isothermal curve are supercritical states. The spinodal zone is delimited by the blue curve, which is the graph of the function g , defined in (24). The saturation dome is represented by the set of red points. Stable states belong to the areas below the critical isothermal curve (in green) and above the saturation dome (in red). The metastable areas correspond to zones above the spinodal zone (in blue) and below the saturation dome (in red).

in the (τ, e) -plane. Actually the construction of the concave hull of the van der Waals entropy function $(\tau, e) \mapsto s$ is equivalent to the Maxwell equal area rule construction [6, 10]. An analogous proof, based on the properties of the Legendre transform, is available in [17]. In practice, the computation of the concave hull of the graph of $(\tau, e) \mapsto s$ boils down to the construction of a ruled surface. For any point (τ, e) , this ruled surface contains a segment which is bitangent to the graph of $(\tau, e) \mapsto s$ in two points denoted (τ_1^*, e_1^*) and (τ_2^*, e_2^*) . The set of points $((\tau_1^*, e_1^*), (\tau_2^*, e_2^*))$ defines the saturation dome in the (τ, e) plane and is represented in red in Figure 2. Note that the computation of the points $((\tau_1^*, e_1^*), (\tau_2^*, e_2^*))$ is not explicit and requires the resolution of a nonlinear system [6, 10, 17]. However if we assume that the set of the red dots is the graph of a function $g^* : \tau \rightarrow g^*(\tau)$, then the curve $(\tau, g^*(\tau))$ defines the saturation dome $Z_{\text{Saturation}}$, that is

$$(25) \quad Z_{\text{Saturation}} := \{(\tau, e) \in D_s; e = g^*(\tau)\}.$$

Thus the metastable states $Z_{\text{Metastable}}$ corresponds to the states belonging to the saturation domain but outside the spinodal zone

$$(26) \quad Z_{\text{Metastable}} := \{(\tau, e) \in D_s; g(\tau) < e < g^*(\tau)\}.$$

Finally the stable zones, either stable liquid or stable vapor states, correspond to states below the critical isotherm curve and above the saturation dome

$$(27) \quad Z_{\text{Stable}} := \{(\tau, e) \in D_s; g^*(\tau) < e < e(\tau, T_c)\}.$$

3. THERMODYNAMICS OF EQUILIBRIA FOR A MULTICOMPONENT SYSTEM

We consider a system of mass $M > 0$, volume $V > 0$ and energy $E > 0$ which is composed of I subsystems. Each subsystem $i = 1, \dots, I$ is characterized by its mass $M_i \geq 0$, its volume $V_i \geq 0$ and its energy $E_i \geq 0$. Moreover, we assume that each subsystem i follows the same non concave entropy $S(M_i, V_i, E_i)$, namely the van der Waals EoS in its extensive setting. The conservations of mass and energy require that

$$(28) \quad M = \sum_{i=1}^I M_i, \quad E = \sum_{i=1}^I E_i.$$

Furthermore, we suppose that all the subsystems are immiscible and that no vacuum appears, in the sense that

$$(29) \quad V = \sum_{i=1}^I V_i.$$

The entropy of the system is the sum of the partial entropies of each subsystem:

$$(M_i, V_i, E_i)_{i=1, \dots, I} \mapsto \sum_{i=1}^I S(M_i, V_i, E_i).$$

According to the second principle of thermodynamics, the entropy of the multicomponent system achieves its maximum at Thermodynamic equilibrium. Considering a state vector (M, V, E) of the multicomponent system, the equilibrium entropy is

$$(30) \quad \Sigma(M, V, E) = \sup_{(M_i, V_i, E_i) \in (\mathbb{R}^+)^3} \sum_{i=1}^I S(M_i, V_i, E_i),$$

under the constraints (28)-(29).

We now turn to the intensive formulation of the maximization problem. In the following, we denote $\varphi_i = M_i/M \in [0, 1]$ the mass fraction, $\alpha_i = V_i/V \in [0, 1]$ the volume fraction and $\xi_i = E_i/E \in [0, 1]$ the energy fraction. Given $\tau = V/M$ and $e = E/M$ the specific volume and specific energy of the multicomponent system, the specific volume of the subsystem $i = 1, \dots, I$ is $\tau_i = V_i/M_i = \alpha_i \tau / \varphi_i \geq 0$ and its specific energy is $e_i = E_i/M_i = \xi_i e / \varphi_i \geq 0$.

The conservation of mass and energy and the volume constraints read now

$$(31) \quad \sum_{i=1}^I \varphi_i = 1, \quad \sum_{i=1}^I \varphi_i \tau_i = \tau, \quad \sum_{i=1}^I \varphi_i e_i = e.$$

Using the homogeneity property of the extensive entropy function S , the definitions of the mass fractions φ_i and phasic intensive quantities τ_i and e_i , the intensive form of the equilibrium entropy of the system is, for any state vector (τ, e)

$$(32) \quad \sigma(\tau, e) = \sup_{(\tau_i, e_i) \in (\mathbb{R}^+)^2} \sum_{i=1}^I \varphi_i s(\tau_i, e_i),$$

under the constraints (31).

3.1. The Gibbs phase rule. For the moment the number I of subsystems, potentially present at the thermodynamic equilibrium, is not determined. Actually the theorem of Caratheodory gives a first estimate on the number of subsystems I . We recall the theorem statement and refer to [25, 18] for a detailed proof.

Theorem 1. (*Theorem of Caratheodory*) *Let A be a subset in \mathbb{R}^n and $\text{conv}(A)$ the set of all the convex combinations of elements of A . Then every point $x \in \text{conv}(A)$ can be represented as a convex combination of $(n + 1)$ points of A .*

In the present context, the theorem provides the following first bound.

Proposition 1. *Consider the maximization problem (32) under the constraints (31). The number of subsystems which may coexist at equilibrium is $I \leq 3$.*

Proof. Consider $(\tau, e) \in (\mathbb{R}^+)^2 \mapsto -s(\tau, e) \in \mathbb{R}$. According to Caratheodory's theorem, the convex hull of the epigraph of $-s$ at any point $(\tau, e) \in (\mathbb{R}^+)^2$ is

$$(33) \quad (\text{conv}(-s))(\tau, e) = \inf \sum_{i=1}^3 -\lambda_i s(\tau_i, e_i),$$

with $\sum_{i=1}^3 \lambda_i \tau_i = \tau$ and $\sum_{i=1}^3 \lambda_i e_i = e$ where the infimum is taken over all the expressions of (τ, e) as a convex combinations of three points (τ_i, e_i) , $i = 1, 2, 3$. Now considering $\lambda_i = \varphi_i$, we recover the intensive constraints (31) and the maximization problem (32) is equivalent to the determination of the concave hull of s . \square

As a consequence of Caratheodory's Theorem, at the most three phases remain at thermodynamic equilibrium. This result is in total agreement with the Gibbs phase rule. Indeed, considering a single component system, the Gibbs phase rule states that the number of phases is $I = 3 - F$, where $F \geq 0$ is the degree of freedom [2, 24].

Actually when considering the van der Waals EoS, the admissible number of subsystems present at Thermodynamic equilibrium restricts to at most 2.

Theorem 2. *Consider the maximization problem (32), and assume that the entropy function s verifies the inequality (18). Then*

$$(34) \quad I(\tau, e) < 3 \quad \forall (\tau, e) \in D_s.$$

Proof. Assume that $I = 3$ and consider a point $X \in D_s$. Then X belongs to a simplex of dimension 2. On the one hand, inside this simplex, the concave hull of s , denoted $\text{conc}(s)$ is an affine function. It follows that the partial derivatives of $\text{conc}(s)$, $\partial_\tau \text{conc}(s)(X)$ and $\partial_e \text{conc}(s)(X)$ are constant. On the other hand, at the boundaries of the simplex, the concave hull $\text{conc}(s)$ is tangent to the surface $(\tau, e) \mapsto s$. Hence $\partial_e \text{conc}(s)(X) = \partial_e s(X)$, which leads to a contradiction with property (18). \square

According to Theorem 2, the maximization process using the van der Waals EoS does not allow the coexistence of more than two phases and prevents from the modelling of a triple point.

3.2. Maxima of the constrained optimization problem. From now on we consider $I = 2$ and consider the optimization problem

$$(35) \quad \sigma(\tau, e) = \max \mathcal{S}(\varphi_1, \varphi_2, \tau_1, \tau_2, e_1, e_2),$$

where

$$(36) \quad \mathcal{S}(\varphi_1, \varphi_2, \tau_1, \tau_2, e_1, e_2) = \varphi_1 s(\tau_1, e_1) + \varphi_2 s(\tau_2, e_2),$$

under the constraints

$$(37) \quad \varphi_1 + \varphi_2 = 1, \quad \varphi_1 \tau_1 + \varphi_2 \tau_2 = \tau, \quad \varphi_1 e_1 + \varphi_2 e_2 = e.$$

Note that if $\rho_1 \neq \rho_2$ and $e_1 \neq e_2$, (37) imply that the mass fractions φ_i , $i = 1, 2$ satisfy

$$(38) \quad \varphi_1 = \frac{\tau - \tau_2}{\tau_1 - \tau_2} = \frac{e - e_2}{e_1 - e_2}, \quad \varphi_2 = \frac{\tau - \tau_1}{\tau_2 - \tau_1} = \frac{e - e_1}{e_2 - e_1}.$$

On the other hand, if $\tau = \tau_1 = \tau_2$ and $e = e_1 = e_2$, the mass fraction is undetermined. In order to preserve the positivity of the fractions, we assume that

$$(39) \quad (\tau, e) \in [\min(\tau_1, \tau_2), \max(\tau_1, \tau_2)] \times [\min(e_1, e_2), \max(e_1, e_2)].$$

Introducing the Lagrange multipliers λ_φ , λ_τ and λ_e associated to the constraints (37), we define the Lagrangian

$$(40) \quad L(\lambda_\varphi, \lambda_\tau, \lambda_e, x) = \mathcal{S}(x) + \lambda_\varphi \beta_\varphi(x) + \lambda_\tau \beta_\tau(x) + \lambda_e \beta_e(x),$$

with $x = (\varphi_1, \varphi_2, \tau_1, \tau_2, e_1, e_2)$ and

$$(41) \quad \begin{cases} \beta_\varphi(x) = \varphi_1 + \varphi_2 - 1, \\ \beta_\tau(x) = \varphi_1 \tau_1 + \varphi_2 \tau_2 - \tau, \\ \beta_e(x) = \varphi_1 e_1 + \varphi_2 e_2 - e. \end{cases}$$

Since \mathcal{S} is C^1 and the conditions (41) are affine, we obtain straightforwardly the optimality conditions for the maxima in the problem (35)-(37):

$$(42a) \quad s(\tau_1, e_1) + \lambda_\varphi + \lambda_\tau \tau_1 + \lambda_e e_1 = 0,$$

$$(42b) \quad s(\tau_2, e_2) + \lambda_\varphi + \lambda_\tau \tau_2 + \lambda_e e_2 = 0,$$

$$(42c) \quad \varphi_1 \frac{p(\tau_1, e_1)}{T(\tau_1, e_1)} + \varphi_1 \lambda_\tau = 0,$$

$$(42d) \quad \varphi_2 \frac{p(\tau_2, e_2)}{T(\tau_2, e_2)} + \varphi_2 \lambda_\tau = 0,$$

$$(42e) \quad \varphi_1 \frac{1}{T(\tau_1, e_1)} + \varphi_1 \lambda_e = 0,$$

$$(42f) \quad \varphi_2 \frac{1}{T(\tau_2, e_2)} + \varphi_2 \lambda_e = 0.$$

We now turn to the determination of the maxima of the problem (35). It turns out that it involves the notion of relative entropy, which is defined, for any two states $a, b \in (\mathbb{R}^+)^2$ by

$$(43) \quad s(a|b) = s(a) - s(b) - \nabla s(b) \cdot (a - b).$$

Proposition 2. *The maxima of the problem (35)-(37) are*

(1) **Identification of phases 1 and 2:**

- $\tau_1 = \tau_2 = \tau$ and $e_1 = e_2 = e$, φ_i undetermined,

• $\varphi_1 = 0, \varphi_2 = 1, (\tau_2, e_2) = (\tau, e)$ and (τ_1, e_1) solution to

$$(44) \quad \begin{cases} s((\tau_1, e_1)|(\tau, e)) &= 0, \\ \mu(\tau_1, e_1)/T(\tau_1, e_1) &= \mu(\tau, e)/T(\tau, e). \end{cases}$$

• $\varphi_1 = 1, \varphi_2 = 0, (\tau_1, e_1) = (\tau, e)$ and (τ_2, e_2) solution to

$$(45) \quad \begin{cases} s((\tau_2, e_2)|(\tau, e)) &= 0, \\ \mu(\tau_2, e_2)/T(\tau_2, e_2) &= \mu(\tau, e)/T(\tau, e). \end{cases}$$

(2) **Saturation states:** there exists a unique couple of points

$M_1^* = (\tau_1^*, e_1^*, s(\tau_1^*, e_1^*))$ and $M_2^* = (\tau_2^*, e_2^*, s(\tau_2^*, e_2^*))$
with $\tau \in [\min(\tau_1^*, \tau_2^*), \max(\tau_1^*, \tau_2^*)]$ and $e \in [\min(e_1^*, e_2^*), \max(e_1^*, e_2^*)]$ given by (38), satisfying

$$(46) \quad \begin{cases} p(\tau_1^*, e_1^*) = p(\tau_2^*, e_2^*), \\ \mu(\tau_1^*, e_1^*) = \mu(\tau_2^*, e_2^*), \\ T(\tau_1^*, e_1^*) = T(\tau_2^*, e_2^*), \end{cases}$$

such that $M = (\tau, e, \sigma(\tau, e))$ belongs to the line segment $(M_1^*, M_2^*) = \{zM_1^* + (1-z)M_2^*, z \in [0, 1]\}$ contained in the concave hull $\text{conc}(s)$.

Proof. The first case $\tau = \tau_1 = \tau_2$ and $e = e_1 = e_2$ is straightforward. We focus on the case $\varphi_1 = 0$. The mass conservation constraint induces $\varphi_2 = 1$ and thus $\tau_2 = \tau$ and $e_2 = e$. Then the optimality conditions (42d) and (42f) give

$$\lambda_\tau = -p(\tau, e)/T(\tau, e), \quad \lambda_e = -1/T(\tau, e).$$

Associated with the conditions (42a) and (42b), the definition of the relative entropy (43) and the definition of the chemical potential (11), one determines (τ_1, e_1) as the solution of (44). The same holds for the case $\varphi_1 = 1$.

We now consider the saturation case. It is characterized by $\varphi_1\varphi_2 \neq 0$. The optimization procedure also reads as a convexification of $(\tau, e) \mapsto s(\tau, e)$ in the sense that the graph of $(\tau, e) \mapsto \sigma(\tau, e)$ is the concave hull of $(\tau, e) \mapsto s(\tau, e)$, see the definition (33). Then for any saturation state (τ, e) , the graph of σ contains a segment $(M_1^*M_2^*)$ passing through $(\tau, e, \sigma(\tau, e))$. The characterization (46) of the points M_1^* and M_2^* derives from the optimality conditions. Combining (42e) and (42f) gives the temperatures equality

$$\frac{1}{T(\tau_1, e_1)} = \frac{1}{T(\tau_2, e_2)}.$$

Similarly using (42c) and (42d), yields

$$\frac{p(\tau_1, e_1)}{T(\tau_1, e_1)} = \frac{p(\tau_2, e_2)}{T(\tau_2, e_2)}.$$

Finally (42a) and (42b), combined with the definition of the chemical potential (11), give

$$\frac{\mu(\tau_1, e_1)}{T(\tau_1, e_1)} = \frac{\mu(\tau_2, e_2)}{T(\tau_2, e_2)}.$$

We now address the uniqueness of the segment $(M_1^*M_2^*)$. Outside the spinodal zone, the van der Waals entropy is a concave and increasing function with respect to τ and e . Then there is a bijection between (p, T) and (τ_i, e_i) , $i = 1, 2$. Define $\widetilde{M}_1^* = (\widetilde{\tau}_1^*, \widetilde{e}_1^*)$ and $\widetilde{M}_2^* = (\widetilde{\tau}_2^*, \widetilde{e}_2^*)$. If $(\tau, \sigma(\tau, e)) \in (M_1^*M_2^*) \cap (\widetilde{M}_1^*\widetilde{M}_2^*)$, since (p, T, μ) are

constant along $(M_1^* M_2^*)$ and $(\widetilde{M}_1^* \widetilde{M}_2^*)$, then $M_i^* = \widetilde{M}_i^*$ and the segments coincide. \square

Notice that, for a given saturation state (τ, e) , the quadruplet $(\tau_1^*, \tau_2^*, e_1^*, e_2^*)$ satisfies also

$$(47) \quad s((\tau_1^*, e_1^*) | (\tau_2^*, e_2^*)) = s((\tau_2^*, e_2^*) | (\tau_1^*, e_1^*)) = 0.$$

We emphasize that the necessary conditions in Proposition 2 include all equilibrium states, regardless of their stability. In particular we recover in item (1) the complete van der Waals EoS, including physically unstable states (spinodal zone), and liquid and vapor metastable and stable states.

To proceed further the classical method consists in studying the local concavity of the mixture entropy out equilibrium \mathcal{S} introduced in (36). We adopt here the approach proposed in [22]. We introduce a relaxation towards the equilibrium states by means of a dynamical system.

4. DYNAMICAL SYSTEM AND ATTRACTION BASSINS

The goal of this section is to introduce time dependence to create a dynamical system able to characterize all the equilibrium states including the metastable states. To build the appropriate dynamical system, we impose two basic criteria:

- long-time equilibria coincide with the maxima given by the optimality conditions in Proposition 2.
- the mixture entropy increases along trajectories.

Fix (τ, e) a state vector of the system. The maximization problem applies to six variables under the three constraints (37). Hence it is sufficient to reduce the variables from six to three. We consider the vector of volume, mass and energy fractions $\mathbf{r} = (\alpha, \varphi, \xi)$. Then the phasic specific energies and volumes are now functions of $\mathbf{r} = (\alpha, \varphi, \xi) \in]0, 1[^3$ with

$$(48) \quad \begin{aligned} \tau_1(\mathbf{r}) &= \frac{\alpha\tau}{\varphi}, & \tau_2(\mathbf{r}) &= \frac{(1-\alpha)\tau}{1-\varphi}, \\ e_1(\mathbf{r}) &= \frac{\xi e}{\varphi}, & e_2(\mathbf{r}) &= \frac{(1-\xi)e}{1-\varphi}. \end{aligned}$$

The formulas in (48) do not suggest any natural order in the volumes nor energies. Besides it is possible that the phasic specific volumes (resp. energies) coincide. Indeed, if $\alpha = \varphi = \xi \in]0, 1[$, then $\tau_1(\mathbf{r}) = \tau_2(\mathbf{r}) = \tau$ and $e_1(\mathbf{r}) = e_2(\mathbf{r}) = e$. Hence the constraint (39) still remains.

In this context, the mixture entropy of the system becomes a function of \mathbf{r} , still denoted \mathcal{S} :

$$(49) \quad \mathcal{S}(\mathbf{r}) = \varphi s(\tau_1(\mathbf{r}), e_1(\mathbf{r})) + (1-\varphi)s(\tau_2(\mathbf{r}), e_2(\mathbf{r})).$$

Using the relations (48) and the expressions (9) of the partial derivatives of the entropy function, the gradient of \mathcal{S} reads

$$(50) \quad \nabla_{\mathbf{r}} \mathcal{S}(\mathbf{r}) = \begin{pmatrix} \tau \frac{p(\tau_1(\mathbf{r}), e_1(\mathbf{r}))}{T(\tau_1(\mathbf{r}), e_1(\mathbf{r}))} - \tau \frac{p(\tau_2(\mathbf{r}), e_2(\mathbf{r}))}{T(\tau_2(\mathbf{r}), e_2(\mathbf{r}))} \\ -\frac{\mu(\tau_1(\mathbf{r}), e_1(\mathbf{r}))}{T(\tau_1(\mathbf{r}), e_1(\mathbf{r}))} + \frac{\mu(\tau_2(\mathbf{r}), e_2(\mathbf{r}))}{T(\tau_2(\mathbf{r}), e_2(\mathbf{r}))} \\ \frac{1}{T(\tau_1(\mathbf{r}), e_1(\mathbf{r}))} - \frac{1}{T(\tau_2(\mathbf{r}), e_2(\mathbf{r}))} \end{pmatrix}.$$

Observe that both \mathcal{S} and $\nabla_{\mathbf{r}}\mathcal{S}$ are defined only for $(\alpha, \varphi, \xi) \in]0, 1[^3$.

We wish to construct a dynamical system which complies with the entropy growth criterion in the sense that entropy increases along the trajectories *i.e.* $d/dt\mathcal{S}(\mathbf{r}(t)) \geq 0$. A naive choice is to choose $\dot{\mathbf{r}}$ close to $\nabla_{\mathbf{r}}\mathcal{S}$. We introduce the following dynamical system:

$$(51) \quad \begin{cases} \dot{\alpha}(t) = \alpha(1 - \alpha)\tau \left(\frac{p(\tau_1(\mathbf{r}), e_1(\mathbf{r}))}{T(\tau_1(\mathbf{r}), e_1(\mathbf{r}))} - \frac{p(\tau_2(\mathbf{r}), e_2(\mathbf{r}))}{T(\tau_2(\mathbf{r}), e_2(\mathbf{r}))} \right), \\ \dot{\varphi}(t) = \varphi(1 - \varphi) \left(\frac{\mu(\tau_2(\mathbf{r}), e_2(\mathbf{r}))}{T(\tau_2(\mathbf{r}), e_2(\mathbf{r}))} - \frac{\mu(\tau_1(\mathbf{r}), e_1(\mathbf{r}))}{T(\tau_1(\mathbf{r}), e_1(\mathbf{r}))} \right), \\ \dot{\xi}(t) = \xi(1 - \xi)e \left(\frac{1}{T(\tau_1(\mathbf{r}), e_1(\mathbf{r}))} - \frac{1}{T(\tau_2(\mathbf{r}), e_2(\mathbf{r}))} \right). \end{cases}$$

Proposition 3. *The dynamical system (51) satisfies the following properties.*

- (1) *If $\mathbf{r}(0) \in]0, 1[^3$ then, for all time $t > 0$, one has $\mathbf{r}(t) \in]0, 1[^3$.*
- (2) *If the condition (39) is satisfied at $t = 0$, then (τ, e) belongs to the segment $[(\tau_1(\mathbf{r}), e_1(\mathbf{r}))(t), (\tau_2(\mathbf{r}), e_2(\mathbf{r}))(t)]$ for all time $t > 0$.*
- (3) *The mixture entropy increases along the trajectories*

$$(52) \quad \frac{d}{dt}\mathcal{S}(\mathbf{r}(t)) \geq 0.$$

Proof. The multiplicative term $\alpha(1 - \alpha)$ in the first equation of (51) ensures that the right-hand side vanishes if $\alpha = 0$ or $\alpha = 1$. The same holds for the equations on the remaining fractions φ and ξ . This proves (1). Item (2) is nothing but a reformulation of (38). Finally, the time derivative of the mixture entropy writes

$$\frac{d}{dt}\mathcal{S}(\mathbf{r}(t)) = \nabla\mathcal{S}(\mathbf{r}) \cdot \dot{\mathbf{r}}(t).$$

Since $\tau > 0$, $e > 0$ and the fractions belong to $]0, 1[$, it follows that the item (3) holds true. \square

4.1. Equilibria and attractivity. In the sequel, we let $\mathbb{F}(\mathbf{r}) = (\mathbb{F}^\alpha, \mathbb{F}^\varphi, \mathbb{F}^\xi)$ be the right-hand side of (51), such that

$$(53) \quad \begin{cases} \dot{\alpha}(t) = \mathbb{F}^\alpha(\mathbf{r}), \\ \dot{\varphi}(t) = \mathbb{F}^\varphi(\mathbf{r}), \\ \dot{\xi}(t) = \mathbb{F}^\xi(\mathbf{r}). \end{cases}$$

Proposition 4 (Equilibrium states). *The equilibrium states for the dynamical system (51) are*

- (1) *saturation states: either $\mathbf{r}^* = (\alpha^*, \varphi^*, \xi^*)$ or $\mathbf{r}^\# = (1 - \alpha^*, 1 - \varphi^*, 1 - \xi^*)$, with $\alpha^* \neq \varphi^* \neq \xi^* \in]0, 1[$, defined by (48) such that $\tau_i^* = \tau_i(\mathbf{r}^*) = \tau_i(\mathbf{r}^\#)$ and $e_i^* = e_i(\mathbf{r}^*) = e_i(\mathbf{r}^\#)$, $i = 1, 2$, corresponding to the characterization (46) of Proposition 2- (2).*
- (2) *Identification of phases 1 and 2: $\bar{\mathbf{r}} = (\beta, \beta, \beta)$, $\beta \in]0, 1[$ such that $\tau_1(\bar{\mathbf{r}}) = \tau_2(\bar{\mathbf{r}}) = \tau$ and $e_1(\bar{\mathbf{r}}) = e_2(\bar{\mathbf{r}}) = e$.*

The equilibria of the dynamical system are given by $\mathbb{F}(\mathbf{r}) = 0$. In the case of equilibria (1), consider that $\alpha \neq \varphi \neq \xi$. Then, according to the Proposition 2- (2), there exists a unique triplet $r^* = (\alpha^*, \varphi^*, \xi^*)$ such that the characterization (46) holds. It turns out that $\mathbf{r}^\#$ is also an equilibrium of the system. If the equilibrium r^* corresponds to $\tau_1^* < \tau < \tau_2^*$, $e_1^* < e < e_2^*$, then the equilibrium $\mathbf{r}^\#$ corresponds to

$\tau_1^* > \tau > \tau_2^*$ and $e_1^* > e > e_2^*$ and conversely. In the case of equilibria (2), the two phases coincide, in the sense that $\tau_1 = \tau_2 = \tau$ and $e_1 = e_2 = e$. The determination of the constant $\beta \in]0, 1[$ depends on the initial data of the dynamical system (51). We emphasize that the equilibrium states $\mathbf{r} = (\beta, \beta, \beta)$ are valid for all states (τ, e) and go over the van der Waals surface.

To go further and identify the physically admissible equilibrium states, we must investigate their stability and attractivity.

Proposition 5 (Attractivity). *The equilibrium states are classified as follow:*

- The saturation states $\mathbf{r}^* = (\alpha^*, \varphi^*, \xi^*)$ and $\mathbf{r}^\# = (1 - \alpha^*, 1 - \varphi^*, 1 - \xi^*)$ are attractive points,
- The equilibrium $\bar{\mathbf{r}} = (\beta, \beta, \beta) \in]0, 1[$, corresponding to the identification of the two phases, is strongly degenerate.

Proof. In the sequel and for sake of readability, we denote $p_i := p(\tau_i(\mathbf{r}), e_i(\mathbf{r}))$, $T_i := T(\tau_i(\mathbf{r}), e_i(\mathbf{r}))$ and $\mu_i := \mu(\tau_i(\mathbf{r}), e_i(\mathbf{r}))$. The goal now is to find the spectrum of the Jacobian matrix of \mathbb{F} denoted by

$$D_{\mathbf{r}}\mathbb{F}(\mathbf{r}) := \begin{pmatrix} \partial_{\alpha}\mathbb{F}^{\alpha}(\mathbf{r}) & \partial_{\varphi}\mathbb{F}^{\alpha}(\mathbf{r}) & \partial_{\xi}\mathbb{F}^{\alpha}(\mathbf{r}) \\ \partial_{\alpha}\mathbb{F}^{\varphi}(\mathbf{r}) & \partial_{\varphi}\mathbb{F}^{\varphi}(\mathbf{r}) & \partial_{\xi}\mathbb{F}^{\varphi}(\mathbf{r}) \\ \partial_{\alpha}\mathbb{F}^{\xi}(\mathbf{r}) & \partial_{\varphi}\mathbb{F}^{\xi}(\mathbf{r}) & \partial_{\xi}\mathbb{F}^{\xi}(\mathbf{r}) \end{pmatrix}.$$

First consider the equilibrium $\bar{\mathbf{r}} = (\beta, \beta, \beta) \in]0, 1[^3$, which corresponds to the identification of the two phases. In that case, the Jacobian matrix $D_{\mathbf{r}}\mathbb{F}(\bar{\mathbf{r}})$ reads

(54)

$$D_{\mathbf{r}}\mathbb{F}(\bar{\mathbf{r}}) = \begin{pmatrix} \tau \partial_{\tau}(\frac{p}{T})(\tau, e) & -\tau \partial_{\tau}(\frac{p}{T})(\tau, e) - e \partial_e(\frac{p}{T})(\tau, e) & e \partial_e(\frac{p}{T})(\tau, e) \\ -\tau \partial_{\tau}(\frac{\mu}{T})(\tau, e) & \tau \partial_{\tau}(\frac{\mu}{T})(\tau, e) + e \partial_e(\frac{\mu}{T})(\tau, e) & -e \partial_e(\frac{\mu}{T})(\tau, e) \\ \tau \partial_{\tau}(\frac{1}{T})(\tau, e) & -\tau \partial_{\tau}(\frac{1}{T})(\tau, e) - e \partial_e(\frac{1}{T})(\tau, e) & e \partial_e(\frac{1}{T})(\tau, e) \end{pmatrix}.$$

Since the middle column is the sum of the two remaining columns, then the determinant of $D_{\mathbf{r}}\mathbb{F}(\bar{\mathbf{r}})$ is zero and the Jacobian matrix admits a null eigenvalue. Hence the equilibrium $\bar{\mathbf{r}}$ is a strongly degenerate.

As the saturation equilibrium $\mathbf{r}^* = (\alpha^*, \varphi^*, \xi^*)$ is concerned, the coefficients of the Jacobian matrix $D_{\mathbf{r}}\mathbb{F}(\mathbf{r}^*)$ do not simplify much and obtaining an explicit formulation of its eigenvalues is out of reach. So, we turn to the numerical illustration of the spectrum $\{\lambda_1, \lambda_2, \lambda_3\}$ of the matrix $D_{\mathbf{r}}\mathbb{F}(\mathbf{r}^*)$ for some saturation states $\mathbf{r}^* = (\alpha^*, \varphi^*, \xi^*)$ with the van der Waals EoS with parameters (20).

\mathbf{r}^*	(τ, e)	(τ_1^*, e_1^*)	(τ_2^*, e_2^*)	λ_1	λ_2	λ_3
(0.71, 0.29, 0.39)	(1.99, 2.1)	(4.76, 2.80)	(0.82, 1.80)	-8.443	-1.290	-0.061
(0.94, 0.73, 0.82)	(3.9, 2.49)	(5.13, 2.77)	(0.81, 1.73)	-5.713	2.048	-0.055
(0.76, 0.22, 0.35)	(2.39, 1.59)	(8.23, 2.56)	(0.73, 1.32)	-8.477	-2.835	-0.110
(0.64, 0.14, 0.24)	(1.79, 1.49)	(8.25, 2.56)	(0.73, 1.32)	-9.044	-2.405	-0.097
(0.68, 0.25, 0.35)	(1.89, 1.99)	(5.11, 2.77)	(0.81, 1.73)	-8.660	-1.368	-0.065

One observes numerically that, for these saturation equilibria \mathbf{r}^* , the Jacobian matrix $D_{\mathbf{r}}\mathbb{F}(\mathbf{r}^*)$ admits three negative eigenvalues, which means that these equilibria are attractive. The same hold true for the equilibrium $\mathbf{r}^\#$. \square

To complete the study of equilibrium states, in particular to cope with the degenerate state $\bar{\mathbf{r}}$, corresponding to the identification of the two phases, we investigate

the attraction basins of $\bar{\mathbf{r}}$, \mathbf{r}^* and $\mathbf{r}^\#$. We introduce the following functions with index I for Identification and S for Saturation:

$$(55) \quad \begin{aligned} G_S(\mathbf{r}) &= -\mathcal{S}(\mathbf{r}) + \text{conc}(s)(\tau, e), \\ G_I(\mathbf{r}) &= -\mathcal{S}(\mathbf{r}) + s(\tau, e), \end{aligned}$$

where $(\text{concs})(\tau, e)$ refers to the concave hull of the function s , see the definition (33).

Proposition 6. *The basins of attraction of the equilibrium states are the following:*

- In the spinodal zone, with $(\tau, e) \in Z_{\text{Spinodal}}$, G_S is a Lyapunov function on the whole domain $(\alpha, \varphi, \xi) \in]0, 1[^3$.
- In the liquid or vapor stable zones, with $(\tau, e) \in Z_{\text{Stable}}$, G_I is a Lyapunov function of the whole domain $(\alpha, \varphi, \xi) \in]0, 1[^3$.

Proof. The two functions are candidate to be a Lyapunov function, since

$$(56) \quad \begin{aligned} &\bullet \text{ by construction } G_S(\mathbf{r}^*) = 0. \text{ Indeed, denoting } p^* = p(\tau_1^*, e_1^*) = p(\tau_1^*, e_2^*), \\ &T^* = T(\tau_1^*, e_1^*) = T(\tau_1^*, e_2^*), \text{ and } \mu^* = \mu(\tau_1^*, e_1^*) = \mu(\tau_1^*, e_2^*), \text{ one has} \\ &G_S(\mathbf{r}^*) = -\varphi^* s(\tau_1^*, e_1^*) - (1 - \varphi^*) s(\tau_2^*, e_2^*) + p^*/T^* \tau + e/T^* + \mu^*/T^* \\ &= p^*/T^* (\tau - \varphi^* \tau_1^* - (1 - \varphi^*) \tau_2^*) + 1/T^* (e - \varphi^* e_1^* - (1 - \varphi^*) e_2^*) \\ &\quad + \mu^*/T^* (1 - \varphi^* - (1 - \varphi^*)) \\ &= 0, \end{aligned}$$

using the Gibbs relation (11). The same holds for the equilibrium $\mathbf{r}^\#$. Similarly $G_I(\bar{\mathbf{r}}) = 0$;

- it holds $\nabla_{\mathbf{r}} G_S(\mathbf{r}) = \nabla_{\mathbf{r}} G_I(\mathbf{r}) = -\nabla_{\mathbf{r}} \mathcal{S}(\mathbf{r})$. Then we obtain as well $\nabla_{\mathbf{r}} G_S(\mathbf{r}^*) = \nabla_{\mathbf{r}} G_S(\mathbf{r}^\#) = \nabla_{\mathbf{r}} G_S(\bar{\mathbf{r}}) = 0$, according to (50);
- for the same reason, and using (52), we have

$$\frac{d}{dt} G_S(\mathbf{r}(t)) = \frac{d}{dt} G_I(\mathbf{r}(t)) \leq 0.$$

It remains to check the positivity of G_S and G_I in a neighborhood of \mathbf{r}^* , $\mathbf{r}^\#$ and $\bar{\mathbf{r}}$ respectively, depending on the domain the state (τ, e) belongs to.

Saturation with $(\tau, e) \in Z_{\text{Spinodal}}$. By definition of $\text{conc}(s)$, $\text{conc}(s)(\tau, e) > \mathcal{S}(\mathbf{r})$ for $\mathbf{r} \neq \mathbf{r}^*$ (or equivalently $\mathbf{r} \neq \mathbf{r}^\#$). Hence $G_S(\mathbf{r}) > 0$.

Stable states with $(\tau, e) \in Z_{\text{Stable}}$. We make use again of the concave hull of s

$$\begin{aligned} G_I(\mathbf{r}) &= -\varphi s(\alpha/\varphi\tau, \xi/\varphi e) - (1 - \varphi) s((1 - \alpha)/(1 - \varphi)\tau, (1 - \xi)/(1 - \varphi)e) - s(\tau, e) \\ &\geq -\varphi \text{conc}(s)(\alpha/\varphi\tau, \xi/\varphi e) \\ &\quad - (1 - \varphi) \text{conc}(s)((1 - \alpha)/(1 - \varphi)\tau, (1 - \xi)/(1 - \varphi)e) \\ &\quad - s(\tau, e) \\ &\geq -\text{conc}(s)(\alpha/\varphi\tau + (1 - \alpha)/(1 - \varphi)\tau, \xi/\varphi e + (1 - \xi)/(1 - \varphi)e) - s(\tau, e) \\ &= -\text{conc}(s)(\tau, e) - s(\tau, e). \end{aligned}$$

In the liquid or vapor stable zones, (τ, e) belongs to the convex hull of the graph of s , that is $\text{conc}(s)(\tau, e) = s(\tau, e)$. Then $G_I(\mathbf{r}) \geq 0$ and the equality occurs if $\mathbf{r} = \bar{\mathbf{r}}$. \square

When considering the metastable regions with $(\tau, e) \in Z_{\text{Metastable}}$, there are two basins of attraction, numerically illustrated in Section 4.2.3, see Figure 9. Unlike in the spinodal zone, the function G_I is non-negative in a neighborhood of (τ, e) ,

provided that (τ, e) belongs to a zone of strict concavity of s . It means that both $\bar{\mathbf{r}}$ and \mathbf{r}^* are reachable. The two basins of attraction are separated by an unstable manifold, which is difficult to determine theoretically and numerically as well. It is already tough in the isothermal framework, see [22], [13] and [14]. In the latter reference the determination of the basins of the metastable states is more precise, even if it is not explicit, the basins being defined through the application of the implicit function theorem.

4.2. Numerical illustrations. This section provides numerical simulations to illustrate the behavior of the dynamical system (51) and the attraction of each possible equilibrium states studied in Propositions 4 and 6.

The computations correspond to the reduced van der Waals EoS, with parameters (20). Cauchy problems for the system (51) are solved using a BDF method for stiff problems available in the Python ODE-solver package. The numerical results are computed for a large computational time $T_f = 200\text{s}$. For each test case, the state (τ, e) of the total system is picked either in the spinodal zone Z_{Spinodal} , in stable zones Z_{Stable} or in a metastable zones $Z_{\text{Metastable}}$, as depicted in Figure 2. We provide the associated vector field in the (α, φ, ξ) phase space and plot some trajectories in the phase space starting from arbitrary initial state $\mathbf{r}(0)$ in order to illustrate the attractivity of the equilibria. Several complementary trajectories are represented in the planes (τ, e) and (τ, p) .

4.2.1. Spinodal zone. The purpose is to illustrate the fact that, for any initial data $\mathbf{r}(0) \in]0, 1[^3$, if the state (τ, e) belongs to the spinodal zone Z_{Spinodal} , the corresponding attraction points are either \mathbf{r}^* or $\mathbf{r}^\#$, that is the system achieves a saturation state of the saturation dome, see Proposition 6.

We consider the state $(\tau, e) = (2, 2.5)$ belonging to the spinodal zone. The vector field of the dynamical system (51) is represented in Figure 3 by light blue arrows. For some random initial conditions $\mathbf{r}(0) \in]0, 1[^3$ (representing by green or yellow dots), the corresponding trajectories converge either towards the point $\mathbf{r}^* = (\alpha^*, \varphi^*, \xi^*)$ (green lines converging towards the green star) or towards $\mathbf{r}^\# = (1 - \alpha^*, 1 - \varphi^*, 1 - \xi^*)$ (yellow lines converging towards the yellow star). In both case, the asymptotic state corresponds to the unique state (τ_i^*, e_i^*) , $i = 1, 2$, defined by (46), which belongs to the saturation dome, see Proposition 2-(2).

In Figures 4 and 5 are plotted trajectories corresponding to the initial condition

$$(57) \quad \mathbf{r}(0) = (0.2, 0.5, 0.42),$$

which corresponds to a state $(\tau_1(\mathbf{r}), e_1(\mathbf{r}))(0) = (0.8, 2.1)$ belonging to the stable liquid zone with $p_1(0) = 0.2986$, $T_1(0) = 1.1166$ and $\mu_1(0) = 2.561$, and a state $(\tau_2(\mathbf{r}), e_2(\mathbf{r}))(0) = (3.2, 2.9)$ belonging to a metastable vapor state with $p_2(0) = 0.1006$, $T_2(0) = 1.0708$ and $\mu_2(0) = 2.2736$. Focusing on Figure 4-top, the trajectory $(\tau_1(\mathbf{r}), e_1(\mathbf{r}))(t)$ is represented with a dashed magenta line. One observes that the trajectory starts from the magenta subcritical isothermal curve, goes through the stable liquid zone and converges towards a point of the saturation dome, see Figure 4-middle for a zoom of the trajectory. The trajectory $(\tau_2(\mathbf{r}), e_2(\mathbf{r}))(t)$ (dashed orange line) is similar, except that it remains in the metastable vapor zone before converging towards a point of the saturation dome. The saturation asymptotic state is characterized by the fractions

$$(58) \quad \mathbf{r}(T_f) = (0.255, 0.55, 0.47),$$

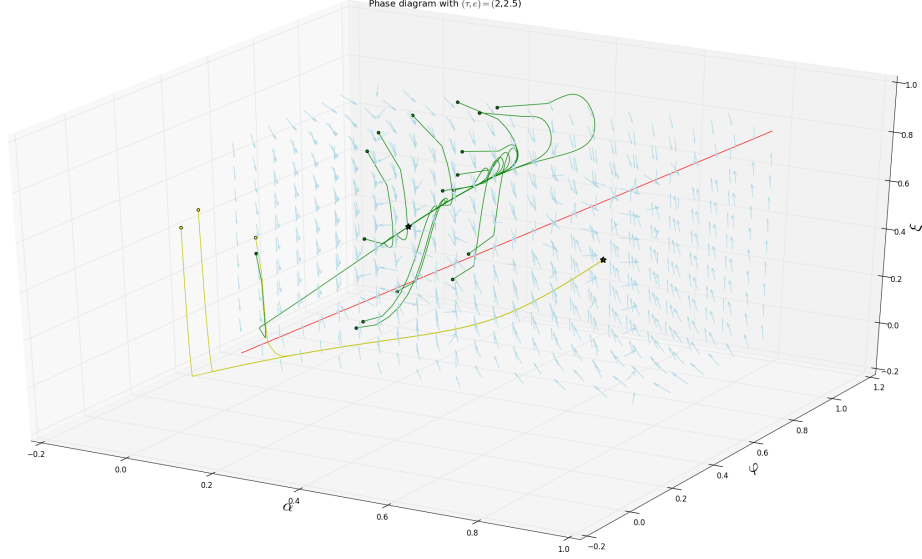


FIGURE 3. Spinodal zone: vector field of the dynamical system (51) (light blue arrows). The red line corresponds to the line $\alpha = \varphi = \xi$. Depending on the initial condition $\mathbf{r}(0)$, the trajectories converge either towards the equilibrium $\mathbf{r}^* = (\alpha^*, \varphi^*, \xi^*)$ (green lines) or towards $\mathbf{r}^\# = (1 - \alpha^*, 1 - \varphi^*, 1 - \xi^*)$ (yellow lines). In both case, the asymptotic regime corresponds to the state (τ_i^*, e_i^*) , $i = 1, 2$, defined by (46), belonging to the saturation dome.

with $(\tau_1, e_1)(T_f) = (0.923, 2.15)$, $(\tau_2, e_2)(T_f) = (3.33, 2.93)$ and $p_1(T_f) = p_2(T_f) = 0.1$, $T_1(T_f) = T_2(T_f) = 1.077$, $\mu_1(T_f) = \mu_2(T_f) = 2.284$. See Figure 4-bottom for a zoom of the trajectory. Figures 5 represent the complementary trajectories plotted in the (τ, p) plane.

4.2.2. *Stable phase zone.* The purpose is to illustrate the attraction of the line $\alpha = \varphi = \xi$ for any initial data $\mathbf{r}(0) \in]0, 1[^3$, as soon as the state (τ, e) belongs to a stable phase zone. The corresponding equilibrium is then the equilibrium $(\tau_1(\bar{\mathbf{r}}), e_1(\bar{\mathbf{r}})) = (\tau_2(\bar{\mathbf{r}}), e_2(\bar{\mathbf{r}})) = (\tau, e)$, see Proposition 6.

We consider a state $(\tau, e) = (3, 3.1)$ belonging to the stable vapor zone. The vector field of the dynamical system (51) is represented in Figure 6 by light blue arrows. For some random initial conditions $\mathbf{r}(0) \in]0, 1[^3$ (represented by green dots), the corresponding trajectories (green lines) converge towards points belonging to the line $\alpha = \varphi = \xi$ plotted in red. Then the asymptotic states are such that $(\tau_1(\bar{\mathbf{r}}), e_1(\bar{\mathbf{r}})) = (\tau_2(\bar{\mathbf{r}}), e_2(\bar{\mathbf{r}})) = (\tau, e)$.

In Figures 7 and 8 are plotted trajectories with the initial condition

$$(59) \quad \mathbf{r}(0) = (0.134, 0.5, 0.338),$$

which corresponds to a state $(\tau_1(\mathbf{r}), e_1(\mathbf{r}))(0) = (0.8, 2.1)$ belonging to the stable liquid zone, and a state $(\tau_2(\mathbf{r}), e_2(\mathbf{r}))(0) = (5.196, 4.1044)$ corresponding to a supercritical state. Focusing on Figure 7, the trajectory $(\tau_1(\mathbf{r}), e_1(\mathbf{r}))(t)$ is represented with a dashed magenta line. One observes that it starts from the magenta

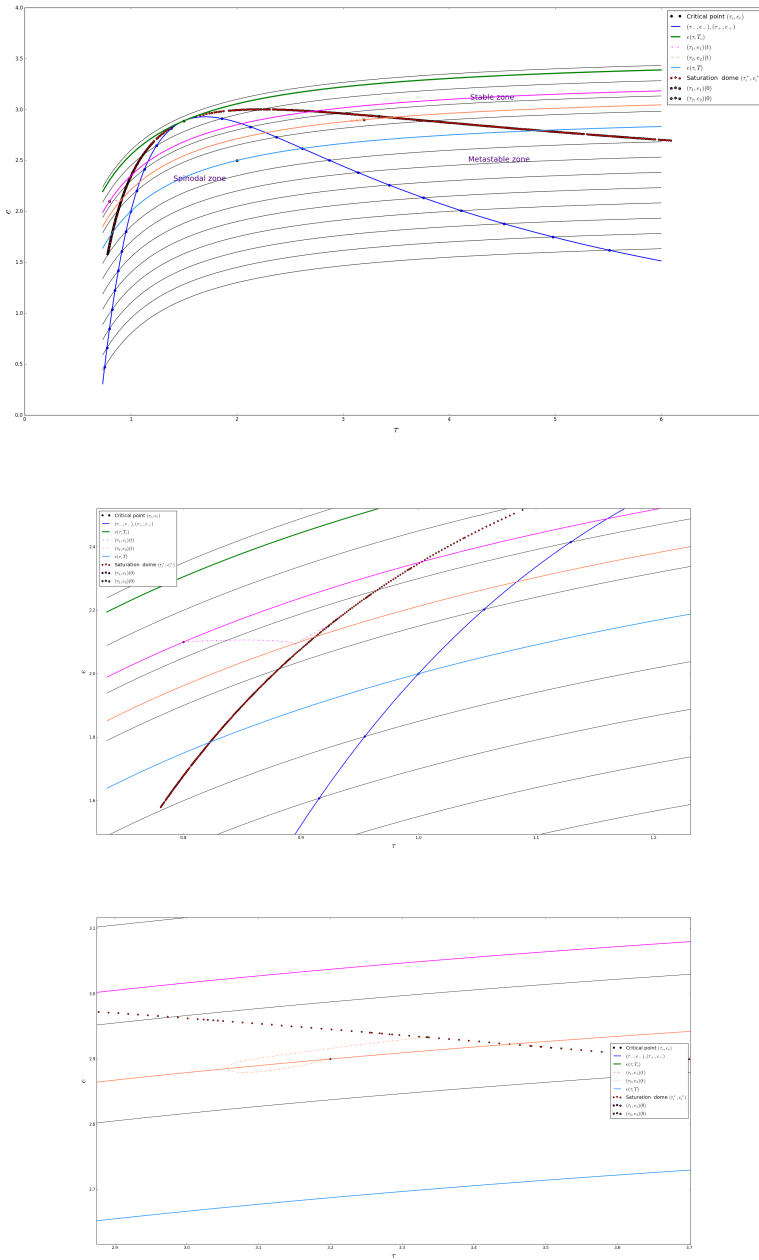


FIGURE 4. Spinodal zone, from top to bottom. Trajectories of the dynamical system (51) in the (τ, e) plane. Starting from an initial state $(\tau_1(\mathbf{r}), e_1(\mathbf{r}))(0)$ in the stable liquid region (on the magenta isothermal curve), the trajectory $(\tau_1(\mathbf{r}), e_1(\mathbf{r}))(t)$ is represented with a dashed magenta line and converges towards the saturation dome. The trajectory $(\tau_2(\mathbf{r}), e_2(\mathbf{r}))(t)$ is represented in orange. Middle and bottom figures: zoom of trajectories $(\tau_1(\mathbf{r}), e_1(\mathbf{r}))(t)$ and $(\tau_2(\mathbf{r}), e_2(\mathbf{r}))(t)$ respectively.

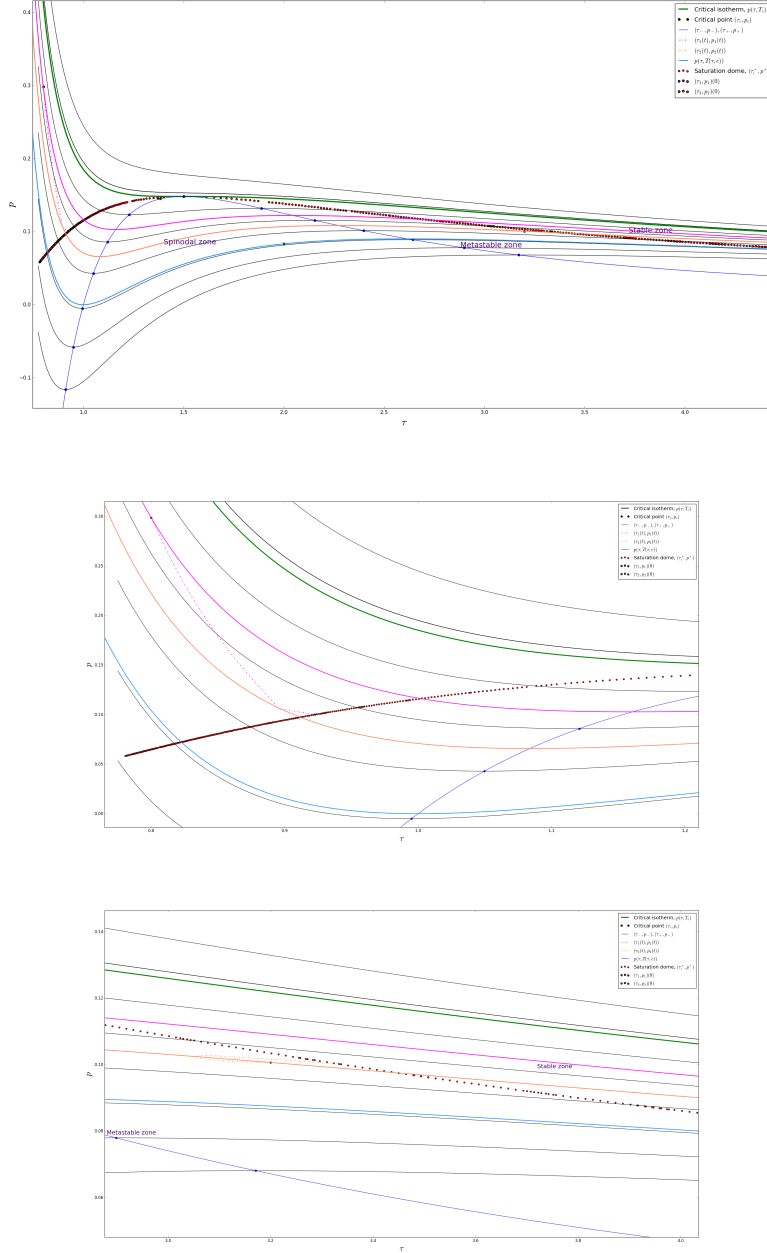


FIGURE 5. Spinodal zone, from top to bottom. Trajectories of the dynamical system (51) in the (τ, p) plane. Starting from an initial state $(\tau_1(\mathbf{r}), p(\tau_1(\mathbf{r}), e_1(\mathbf{r}))(0))$ in the liquid region (on the isothermal curve in magenta), the trajectory $(\tau_1(\mathbf{r}), p(\tau_1(\mathbf{r}), e_1(\mathbf{r}))(t))$ is represented with a dashed magenta line and converges towards the saturation dome. The trajectory $(\tau_2(\mathbf{r}), p(\tau_2(\mathbf{r}), e_2(\mathbf{r}))(t))$ is represented in orange. Middle and bottom figures: zoom of trajectories $(\tau_1(\mathbf{r}), p(\tau_1(\mathbf{r}), e_1(\mathbf{r}))(t))$ and $(\tau_2(\mathbf{r}), p(\tau_2(\mathbf{r}), e_2(\mathbf{r}))(t))$ respectively.

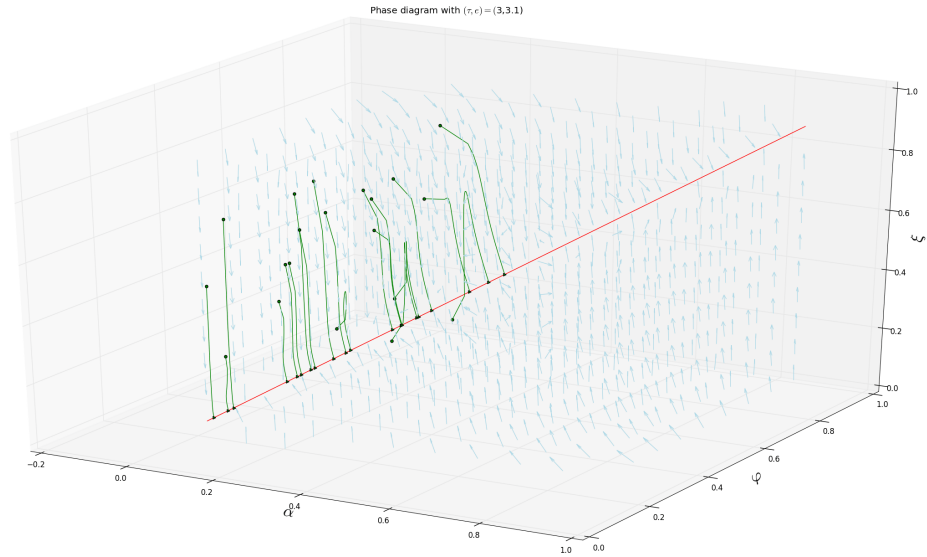


FIGURE 6. Stable phase zone: vector field of the dynamical system (51) (light blue arrows). The red line corresponds to the line $\alpha = \varphi = \xi$. For any initial condition $\mathbf{r}(0)$, the trajectories converge towards a point belonging to the line $\alpha = \varphi = \xi$, corresponding to the state (τ, e) .

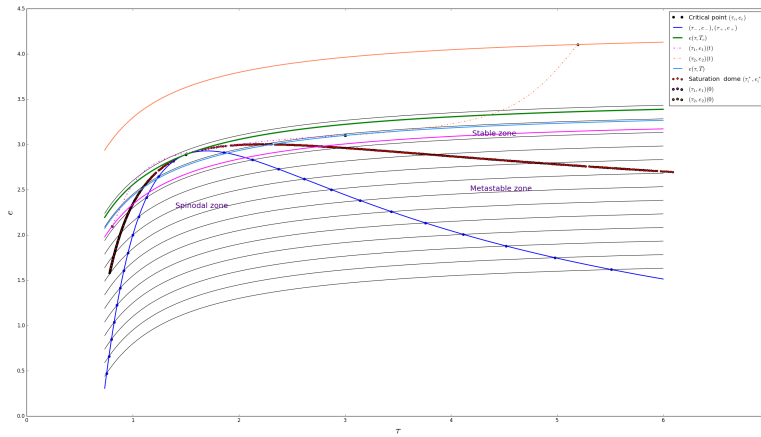


FIGURE 7. Stable phase zone. Trajectories of the dynamical system (51) in the (τ, e) plane. Starting from an initial state $(\tau_1(\mathbf{r}), e_1(\mathbf{r}))(0)$ in the stable liquid region (on the isothermal curve in magenta), the trajectory $(\tau_1(\mathbf{r}), e_1(\mathbf{r}))(t)$ is represented with a dashed magenta line and converges towards the state (τ, e) . The trajectory $(\tau_2(\mathbf{r}(t)), e_2(\mathbf{r}))(t)$ is represented in orange.

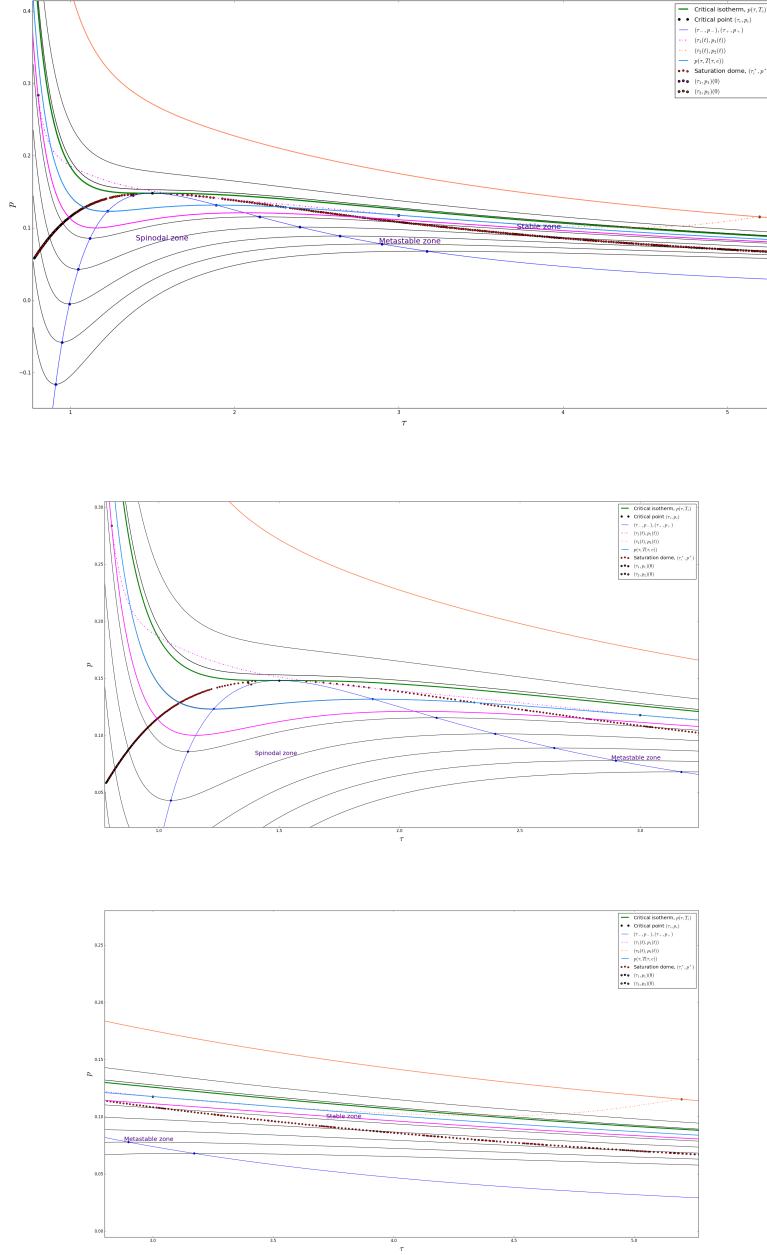


FIGURE 8. Stable phase zone, from top to bottom. Trajectories of the dynamical system (51) in the (τ, p) plane. Starting from an initial state $(\tau_1(\mathbf{r}), p(\tau_1(\mathbf{r}), e_1(\mathbf{r}))) (0)$ in the stable liquid region (on the isothermal curve in magenta), the trajectory $(\tau_1(\mathbf{r}), p(\tau_1(\mathbf{r}), e_1(\mathbf{r}))) (t)$ is represented with a dashed magenta line and converges towards the point (τ, e) . The trajectory $(\tau_2(\mathbf{r}), p(\tau_2(\mathbf{r}), e_2(\mathbf{r}))) (t)$ is represented in orange. Middle and bottom figures: zoom of trajectories $(\tau_1(\mathbf{r}), p(\tau_1(\mathbf{r}), e_1(\mathbf{r}))) (t)$ and $(\tau_2(\mathbf{r}), p(\tau_2(\mathbf{r}), e_2(\mathbf{r}))) (t)$ respectively.

subcritical isothermal curve, goes over the critical point entering the supercritical zone, and finally converges towards the point (τ, e) . The trajectory $(\tau_2(\mathbf{r}), e_2(\mathbf{r}))(t)$ (dashed orange line) is similar, going from the supercritical zone to the stable vapor zone and finally converging towards the point (τ, e) . Figures 5 represent the same trajectories plotted in the (τ, p) plane. One observes that the trajectory of $(\tau_1(\mathbf{r}), p(\tau_1(\mathbf{r}), e_1(\mathbf{r}))) (t)$ starts from the stable liquid zone, crosses the critical isothermal curve twice before converging towards the point $(\tau, p(\tau, e))$.

4.2.3. Metastable zone. The purpose is to illustrate the fact that, if the state (τ, e) belongs to a metastable zone, for any initial data $\mathbf{r}(0) \in]0, 1[^3$, there exist two possible attraction points.

We consider a state $(\tau, e) = (3.2, 2.5)$ belonging to the metastable vapor zone with $p(\tau, e) = 0.0759$ and $T(\tau, e) = 0.9375$. The vector field of the dynamical system (51) is represented in Figure 9 by light blue arrows. For some random initial conditions $\mathbf{r}(0) \in]0, 1[^3$ (represented by green or yellow dots), the complementary trajectories (green or yellow lines) converge towards

- either an attraction point which lies on to the line $\alpha = \varphi = \xi$ (yellow trajectories). In that case the asymptotic state satisfies

$$(\tau_1(\bar{\mathbf{r}}), e_1(\bar{\mathbf{r}})) = (\tau_2(\bar{\mathbf{r}}), e_2(\bar{\mathbf{r}})) = (\tau, e),$$

and remains metastable, see Propositions 2-(1) and 4-(1);

- either the attraction point $\mathbf{r}^* = (\alpha^*, \varphi^*, \xi^*)$ (green trajectories) which concurs with the unique state (τ_i^*, e_i^*) , $i = 1, 2$, defined by (46), which belongs to the saturation dome, see Propositions 2-(2) and 4-(2).

Metastable state and perturbation within the phase. In Figures 10 and 11 the represented trajectories correspond to a realization of the dynamical system for the initial condition

$$(60) \quad \mathbf{r}(0) = (0.5, 0.5, 0.55).$$

It boils down to an initial state $(\tau_1(\mathbf{r}), e_1(\mathbf{r}))(0) = (3.2, 2.75)$ in the metastable vapor zone with $p_1(0) = 0.091$, $T_1(0) = 1.02$, $\mu_1(0) = 2.15$, and to an initial state $(\tau_2(\mathbf{r}), e_2(\mathbf{r}))(0) = (3.2, 2.25)$ belonging to the spinodal zone with $p_2(0) = 0.06$, $T_2(0) = 0.85$, $\mu_2(0) = 1.75$. Notice that in this case, it holds $e_1(\mathbf{r})(0) > e > e_2(\mathbf{r})(0)$. The perturbation is small enough to ensure that the trajectories $(\tau_i(\mathbf{r}), e_i(\mathbf{r}))(t)$ converge towards the point (τ, e) in the metastable zone. The asymptotic state is characterized by the fractions

$$(61) \quad \mathbf{r}(T_f) = (0.499, 0.499, 0.499),$$

with $p_1(T_f) = p_2(T_f) = 0.0759$ and $T_1(T_f) = T_2(T_f) = 0.9374$.

Metastable state and perturbation outside the phase. We provide in Figures 12 and 13 the trajectories of the dynamical system for an initial condition

$$(62) \quad \mathbf{r}(0) = (0.16, 0.5, 0.328).$$

It corresponds to an initial state $(\tau_1(\mathbf{r}), e_1(\mathbf{r}))(0) = (0.8, 2.1)$ in the stable liquid zone and an initial state $(\tau_2(\mathbf{r}), e_2(\mathbf{r}))(0) = (5.376, 3.36)$ belonging to the stable vapor zone. The perturbation is large enough to ensure that the trajectories $(\tau_i(\mathbf{r}), e_i(\mathbf{r}))(t)$ converge towards a state belonging to the saturation dome.

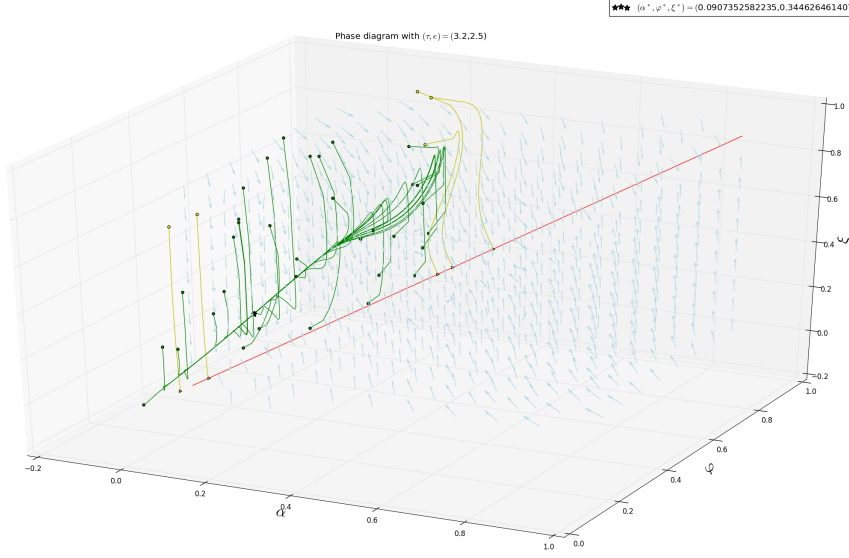


FIGURE 9. Metastable zone: vector field of the dynamical system (51) (light blue arrows). The red line corresponds to the line $\alpha = \varphi = \xi$. For any initial condition $\mathbf{r}(0)$, the trajectories converge either towards a point belonging to the line $\alpha = \varphi = \xi$, corresponding to the state (τ, e) (yellow trajectories), or to the point $\mathbf{r}^* = (\alpha^*, \varphi^*, \xi^*)$, which concurs with a state belonging to the saturation dome (green trajectories).

5. AN HOMOGENEOUS RELAXATION MODEL

The aim of this Section is to investigate the impact of the fluid dynamics on the stability of metastable states and the apparition of phase transition. To do so we now consider the liquid-vapor mixture as a compressible medium. It is described by its density $\rho(t, x)$ (and $\tau(t, x) = 1/\rho(t, x)$ its specific volume), its velocity $u(t, x)$ and its internal energy $e(t, x)$, depending on the time variable $t \in \mathbb{R}^+$ and the one-dimensional space variable $x \in \mathbb{R}$. Since both phases evolve with the same velocity u , we focus on so-called homogeneous models in the spirit of [3, 20].

The homogeneous model reads

$$(63) \quad \begin{cases} \partial_t(\rho\alpha) + \partial_x(\rho u\alpha) = \frac{\rho}{\alpha} \mathbb{F}^\alpha(\mathbf{r}), \\ \partial_t(\rho\varphi) + \partial_x(\rho u\varphi) = \frac{\rho}{\varphi} \mathbb{F}^\varphi(\mathbf{r}), \\ \partial_t(\rho\xi) + \partial_x(\rho u\xi) = \frac{\rho}{\xi} \mathbb{F}^\xi(\mathbf{r}), \\ \partial_t(\rho) + \partial_x(\rho u) = 0, \\ \partial_t(\rho u) + \partial_x(\rho u^2 + p) = 0, \\ \partial_t(\rho E) + \partial_x(\rho u E + up) = 0, \end{cases}$$

where $E = e + u^2/2$ is the total energy. The last three equations correspond to the Euler's system with a mixture pressure law p to be define in the sequel. The first three equations are evolution equations of the fractions $\mathbf{r} = (\alpha, \varphi, \xi) \in]0, 1[^3$,

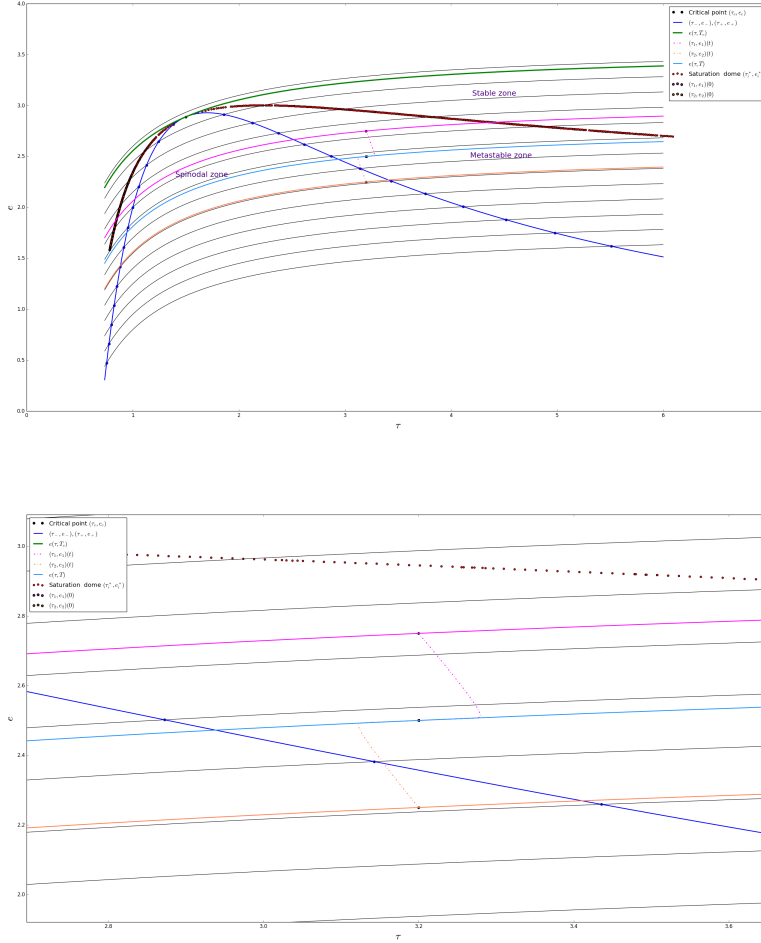


FIGURE 10. Metastable state and perturbation within the phase. Top figure: trajectories of the dynamical system (51) in the (τ, e) plane. Starting from an initial state $(\tau_1(\mathbf{r}), e_1(\mathbf{r}))(0)$ in the metastable vapor region (on the magenta isothermal curve), the trajectory $(\tau_1(\mathbf{r}), e_1(\mathbf{r}))(t)$ is represented with a dashed magenta line and converges towards the state (τ, e) . The trajectory $(\tau_2(\mathbf{r}), e_2(\mathbf{r}))(t)$ is represented in orange and starts with an initial condition in the spinodal zone. Bottom figure: zoom of trajectories $(\tau_i(\mathbf{r}), e_I(\mathbf{r}))(t)$.

with relaxation source terms $(\mathbb{F}^\alpha, \mathbb{F}^\varphi, \mathbb{F}^\xi)$ towards the Thermodynamic equilibrium, which coincide with the dynamical system (51) studied in the previous section. The parameter $\varepsilon > 0$ stands for a relaxation time towards the thermodynamic equilibrium.

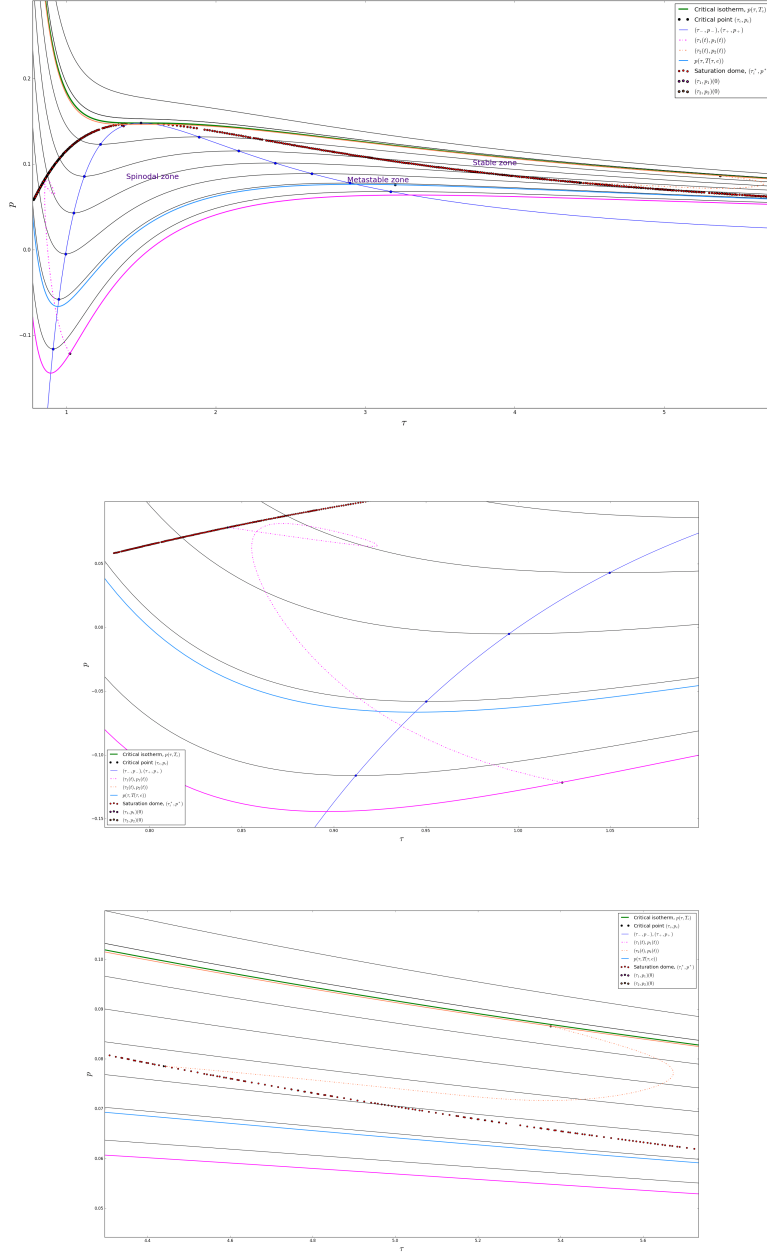


FIGURE 13. Metastable state and perturbation outside the phase. From top to bottom: trajectories of the dynamical system (51) in the (τ, p) plane. Starting from an initial state $(\tau_1(\mathbf{r}), p(\tau_1(\mathbf{r}), e_1(\mathbf{r}))) (0)$ in the stable liquid region (on the magenta isothermal curve), the trajectory $(\tau_1(\mathbf{r}), p(\tau_1(\mathbf{r}), e_1(\mathbf{r}))) (t)$ is represented with a dashed magenta line and converges towards the point (τ, e) . The trajectory $(\tau_2(\mathbf{r}), p(\tau_2(\mathbf{r}), e_2(\mathbf{r}))) (t)$ is represented in orange. Middle and bottom figures: zoom of trajectories $(\tau_1(\mathbf{r}), p(\tau_1(\mathbf{r}), e_1(\mathbf{r}))) (t)$ and $(\tau_2(\mathbf{r}), p(\tau_2(\mathbf{r}), e_2(\mathbf{r}))) (t)$ respectively.

the thermodynamical constraints presented in the previous sections, the considered pressure p is a function of the density ρ , the internal energy e and the fraction vector \mathbf{r} . Following [3, 19, 16, 20], the mixture pressure law should be derived from the mixture entropy function \mathcal{S} defined in (49).

Highlighting the dependency on (τ, e) , the entropy of the mixture reads

$$(64) \quad \mathcal{S}(\tau, e, \mathbf{r}) = \varphi_1 s(\tau_1(\mathbf{r}), e_1(\mathbf{r})) + (1 - \varphi) s(\tau_2(\mathbf{r}), e_2(\mathbf{r})),$$

where s is again the van der Waals EoS and the functions $\tau_i(\mathbf{r})$ and $e_i(\mathbf{r})$ are defined in (48). The associated pressure p and the temperature T of the mixture are deduced from an extended Gibbs relation

$$(65) \quad T d\mathcal{S}(\tau, e, \mathbf{r}) = de + pd\tau + \frac{\partial \mathcal{S}}{\partial \alpha} d\alpha + \frac{\partial \mathcal{S}}{\partial \varphi} d\varphi + \frac{\partial \mathcal{S}}{\partial \xi} d\xi.$$

Then the definitions of the mixture temperature and pressure, as functions of (τ, e, \mathbf{r}) , are

$$(66) \quad \begin{aligned} T(\tau, e, \mathbf{r}) &= \frac{\xi}{T(\tau_1(\mathbf{r}), e_1(\mathbf{r}))} + \frac{1 - \xi}{T(\tau_2(\mathbf{r}), e_2(\mathbf{r}))}, \\ \frac{p(\tau, e, \mathbf{r})}{T(\tau, e, \mathbf{r})} &= \alpha \frac{p(\tau_1(\mathbf{r}), e_1(\mathbf{r}))}{T(\tau_1(\mathbf{r}), e_1(\mathbf{r}))} + (1 - \alpha) \frac{p(\tau_2(\mathbf{r}), e_2(\mathbf{r}))}{T(\tau_2(\mathbf{r}), e_2(\mathbf{r}))}. \end{aligned}$$

The sound speed of the system (63) is

$$(67) \quad c^2 = -\tau^2 \frac{\partial}{\partial \tau} p + \tau^2 p \frac{\partial}{\partial e} p,$$

which, using the expression of the mixture pressure (66), simplifies to

$$(68) \quad \begin{aligned} -\frac{c^2}{T\tau^2} &= \frac{1}{\varphi} (-\alpha, \xi p) H_{s_1} \begin{pmatrix} -\alpha \\ \xi p \end{pmatrix} \\ &+ \frac{1}{1 - \varphi} (-(1 - \alpha), (1 - \xi)p) H_{s_2} \begin{pmatrix} -(1 - \alpha) \\ (1 - \xi)p \end{pmatrix}, \end{aligned}$$

where H_{s_i} denotes the hessian matrix of the phasic entropy $s(\tau_i, e_i)$

$$(69) \quad H_{s_i}(\tau_i, e_i) = \begin{pmatrix} \frac{\partial^2 s}{\partial \tau_i^2} & \frac{\partial^2 s}{\partial \tau_i \partial e_i} \\ \frac{\partial^2 s}{\partial e_i \partial \tau_i} & \frac{\partial^2 s}{\partial e_i^2} \end{pmatrix},$$

and the dependency to the variables has been skipped for readability reasons.

The convective system is hyperbolic if and only if the the right-hand side of (68) is negative. This is the case if the hessian matrices H_{s_1} and H_{s_2} are negative definite, which is true in concavity region of the van der Waals entropy, that is outside the spinodal region Z_{Spinodal} . Hence the system is non-strictly hyperbolic. However, it has been highlighted in [22] in the isothermal context that the domains of hyperbolicity of (63) strongly depend on the attraction basins of the dynamical system (51). More precisely, the invariant domains of hyperbolicity for the relaxed system are subsets of the attraction basins of the dynamical system.

The convective part of the model (63) inherits the wave structure of the Euler system. The fields associated with the fractions \mathbf{r} are linearly degenerated with the eigenvalue u . The momentum and energy conservation laws are genuinely nonlinear fields with velocities $u \pm c$ and the mass equation is linearly degenerated with velocity u .

The Riemann invariants associated to the wave of velocity u are the velocity u and the pressure. Moreover the volume fraction, the mass fraction and the energy fraction are Riemann invariants associated to the genuinely nonlinear waves.

The positivity of the fractions is ensured by both the positivity property of the dynamical system, see Proposition 3-(1), and the form of the convection equations of the fractions \mathbf{r} , see [21].

5.2. Numerical illustrations. Numerous numerical schemes have been proposed for homogeneous models with relaxation, see again [3] and [20] for models involving stiffened gas or tabulated laws. We propose here a very standard approach, and take a special interest to numerical illustrations.

The numerical approximation consists in a fractional step method.

We restrict to regular meshes of size $\Delta x = x_{i+1/2} - x_{i-1/2}$, $i \in \mathbb{Z}$. The time step is $\Delta t = t^{n+1} - t^n$, $n \in \mathbb{N}$. We focus on the convective part of (63) with an initial condition

$$(70) \quad \begin{cases} \partial_t W + \partial_x F(W) = 0, \\ W(0, x) = W_0(x), \end{cases}$$

with $W = (\rho\alpha, \rho\varphi, \rho\xi, \rho, \rho u, \rho E)^T$, and $F(W) = uW + pD$, with $D = (0, 0, 0, 0, 1, u)^T$. Let $W(t^n, x)$ be approximated by

$$(71) \quad w_i^n = \frac{1}{\Delta x} \int_{x_{i-1/2}}^{x_{i+1/2}} W(t^n, x) dx.$$

Integrating the system on the space-time domain $[x_{i-1/2}, x_{i+1/2}] \times [t^n, t^{n+1}]$ provides

$$(72) \quad W_i^{n+1} = W_i^n - \frac{\Delta t}{\Delta x} \left(\mathcal{F}_{i+1/2}^n - \mathcal{F}_{i-1/2}^n \right).$$

We choose the explicit HLLC numerical flux [27] to define the fluxes $\mathcal{F}_{i+1/2}^n$ through the interface $x_{i+1/2} \times [t^n, t^{n+1}]$.

The source terms of the system (63) are accounted for by discretizing

$$(73) \quad \begin{cases} \frac{d}{dt} \rho(t) = 0, & \frac{d}{dt} (\rho\alpha)(t) = \frac{\rho}{\varepsilon} \mathbb{F}_\alpha(\mathbf{r}, \rho, e), \\ \frac{d}{dt} (\rho u)(t) = 0, & \frac{d}{dt} (\rho\varphi)(t) = \frac{\rho}{\varepsilon} \mathbb{F}_\varphi(\mathbf{r}, \rho, e), \\ \frac{d}{dt} (\rho E)(t) = 0, & \frac{d}{dt} (\rho\xi)(t) = \frac{\rho}{\varepsilon} \mathbb{F}_\xi(\mathbf{r}, \rho, e). \end{cases}$$

It can be written in an equivalent manner

$$(74) \quad \begin{cases} \frac{d}{dt} \alpha(t) = \frac{1}{\varepsilon} \mathbb{F}_\alpha(\mathbf{r}(t), \rho(0), e(0)), \\ \frac{d}{dt} \varphi(t) = \frac{1}{\varepsilon} \mathbb{F}_\varphi(\mathbf{r}(t), \rho(0), e(0)), \\ \frac{d}{dt} \xi(t) = \frac{1}{\varepsilon} \mathbb{F}_\xi(\mathbf{r}(t), \rho(0), e(0)). \end{cases}$$

The numerical approximation W^{n+1} is an approximated solution of the system (73) at time $t = \Delta t$ with the initial condition $W^{n+1,*}$ deduced from the convection step.

The numerical method for the convective part has been validated on single-phase test cases with a real van der Waals EoS proposed in [12].

In order to capture accurately the thermodynamic equilibrium, one should ideally consider infinitely fast relaxation with $\varepsilon = 0$. The integration of the source terms

(74) reduces the the the projection of the solution on the appropriate equilibrium (described in Proposition 4), depending on the basin of attraction the state $W^{n+1,*}$ belongs to.

Unfortunately, as mentioned in Section 4.1, the boundaries of the basins of attraction are not explicitly defined. This is for instance the case of the basins of attraction of the spinodal zone and the metastable zones. These basins are either delimited by the saturation dome, which determination requires the resolution of the nonlinear system (46), or by an unstable manifold, which numerical approximation is intrinsically not reachable. Hence we consider in the sequel finite but sufficiently small relaxation time parameter ε coupled with a Runge-Kutta 4 integration method.

Note that in the isothermal case, studied in [14], the determination of the basins of attraction is precise enough to perform infinitely fast relaxation with $\varepsilon = 0$.

5.2.1. *Single-phase test case.* We provide a validation test case which mimics the one proposed in [12], for a non-reduced van der Waals equation of state. The Riemann data correspond to a left stable liquid state and a right stable vapor state, namely

$$(75) \quad \begin{aligned} \rho_L = 1.111, \quad u_L = 0., \quad p_L = 0.2, \quad \alpha_L = \varphi_L = \xi_L = 10^{-6}, \\ \rho_R = 0.277, \quad u_R = 0, \quad p_R = 0.11 \quad \alpha_R = \varphi_R = \xi_R = 10^{-6}. \end{aligned}$$

This test case corresponds to a single-phase subsonic 1-rarefaction wave, since the fractions are constant and small. The domain $[0, 1]$ is decomposed into 500 cells and the discontinuity is applied at $x_0 = 0.5$. The final time of computation is 0.4s and the CFL coefficient is 0.9.

The global behaviour is coherent with the results provided [12]. In particular, the curve profiles around the contact discontinuity is not precise enough. A more robust numerical flux should be considered to overcome the problem, which actually disappears as the grid is refined.

5.2.2. *Interaction of a metastable liquid state and a saturation state.* The test case corresponds to a Riemann problem with a left metastable liquid state and a right saturation state. The initial data are

$$(76) \quad \begin{aligned} \rho_L = 1.25, \quad u_L = 0., \quad p_L = 0.02, \quad \alpha_L = \varphi_L = \xi_L = 0.3, \\ \rho_R = 0.3125, \quad u_R = 0, \quad p_R = 0.0785 \quad \alpha_R = 0.0907, \quad \varphi_R = 0.344, \quad \xi_R = 0.2577. \end{aligned}$$

The right state is at saturation since it holds

$$(77) \quad p_{1,R} = p_{2,R} = 0.0785, \quad T_{1,R} = T_{2,R} = 1.0188, \quad \mu_{1,R} = \mu_{2,R} = 2.102.$$

6. CONCLUSION

This paper concerns the construction of appropriate relaxation source terms towards thermodynamic equilibrium for a liquid-vapor flow with the possible appearance of metastable states. Extending the works [22, 14] in the isothermal context, the two phases are assumed to follow the same non convex van der Waals equation of state. We provide time evolution equations of the fractions of volume, mass and energy of one of the phases which guarantee the growth of the mixture entropy. The dynamical model admits two major properties. First the attractive equilibria are either saturation states, characterized by the equalities of the phasic pressures,

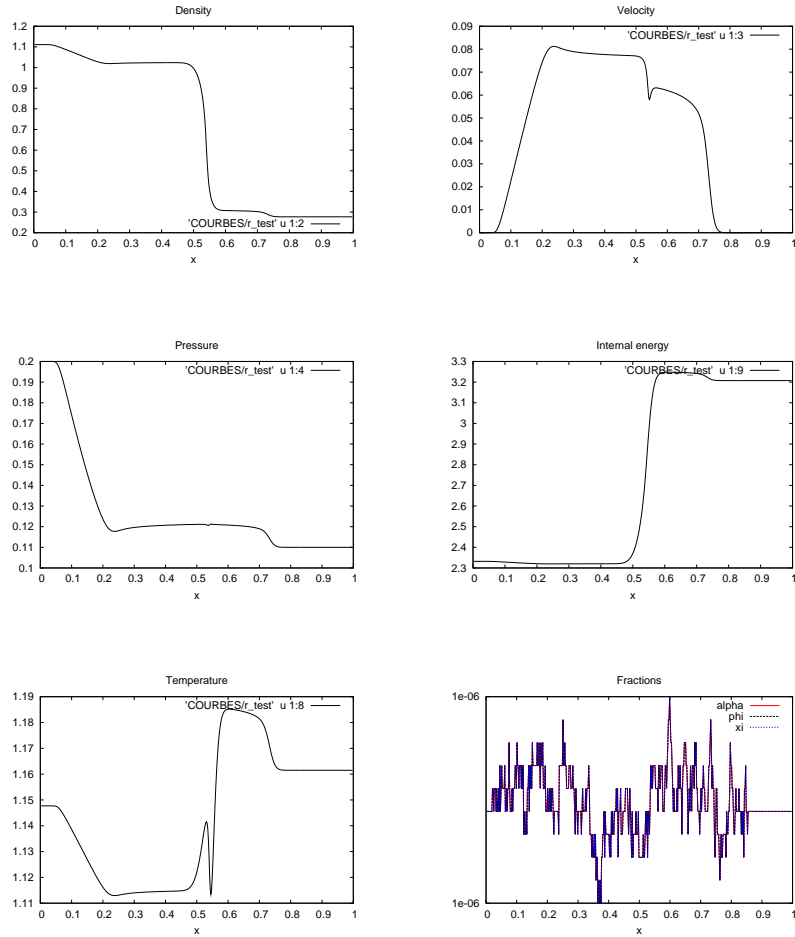


FIGURE 14. Sod test case. From top left to bottom right: density profile, velocity, pressure, internal energy, temperature and fractions profile with respect to the space variable.

temperatures and chemical potential, or stable or metastable states, for which the two phases identify. In the latter case, the equilibrium corresponds to the equality of the fractions to an asymptotic value between 0 and 1 strictly. The fluid is either in a liquid or vapor, metastable or stable, state, but the fractions do not cancel, as it is classically the case in the Baer-Nunziato type model. Second, when considering a mixture state belonging to a metastable zone, there are two possible equilibria depending the initial condition on the fractions. The system reaches either a saturation state or converges toward the metastable initial state characterized by the identification of the two phases. In contrast with standard models, this does not correspond to volume fractions equal to 0 or 1. The method we propose here should be extended to more realistic non convex equations of state. Using tabulated laws could be a real issue because of the difficulty of determining the attraction basins.

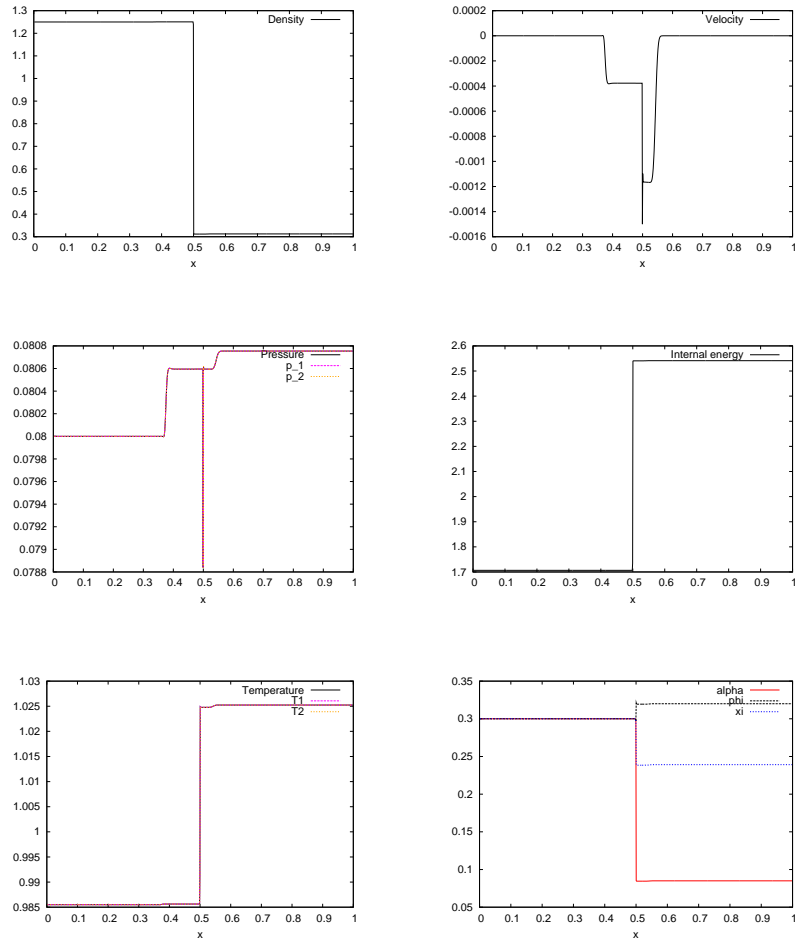


FIGURE 15. Interaction of a metastable liquid and a saturation state. From top left to bottom right: density profile, velocity, pressure, internal energy, temperature and fractions profile with respect to the space variable.

Another issue is the coupling with fluid dynamics, which is merely illustrated here. It deserves a more careful study, from both theoretical and numerical viewpoints.

REFERENCES

- [1] M. R. Baer and J. W. Nunziato. A two phase mixture theory for the deflagration to detonation (ddt) transition in reactive granular materials. *Int. J. Multiphase Flow*, 12(6):861–889, 1986.
- [2] D. W. Ball. *Physical Chemistry*. Cengage Learning, 2002., 2011.
- [3] T. Barberon and P. Helluy. Finite volume simulation of cavitating flows. *Computers and Fluids*, 34(7):832–858, 2005.
- [4] J. Bartak. A study of the rapid depressurization of hot water and the dynamics of vapour bubble generation in superheated water. *Int. J. Multiph. Flow*, 16(5):789–98, 1990.

- [5] H. B. Callen. *Thermodynamics and an introduction to thermostatistics, second edition*. Wiley and Sons, 1985.
- [6] F. Caro. *Modélisation et simulation numérique des transitions de phase liquide vapeur*. PhD thesis, Ecole Polytechnique X, 2004.
- [7] M. De Lorenzo. *Modelling and numerical simulation of metastable two-phase flows*. Theses, Université Paris-Saclay, May 2018.
- [8] M. De Lorenzo, Ph. Lafon, M. Di Matteo, M. Pelanti, J.-M. Seynhaeve, and Y. Bartosiewicz. Homogeneous two-phase flow models and accurate steam-water table look-up method for fast transient simulations. *Int. J. Multiph. Flow*, 95:199–219, 2017.
- [9] M. De Lorenzo, Ph. Lafon, and M. Pelanti. A hyperbolic phase-transition model with non-instantaneous EoS-independent relaxation procedures. *J. Comput. Phys.*, 379:279–308, 2019.
- [10] G. Faccanoni, S. Kokh, and G. Allaire. Modelling and simulation of liquid-vapor phase transition in compressible flows based on thermodynamical equilibrium. *ESAIM Math. Model. Numer. Anal.*, 46(5):1029–1054, 2012.
- [11] S. Fechter, C.-D. Munz, C. Rohde, and C. Zeiler. A sharp interface method for compressible liquid-vapor flow with phase transition and surface tension. *J. Comput. Phys.*, 336:347–374, 2017.
- [12] T. Gallouët, J.-M. Hérard, and N. Seguin. Some recent finite volume schemes to compute Euler equations using real gas EOS. *Internat. J. Numer. Methods Fluids*, 39(12):1073–1138, 2002.
- [13] Hala Ghazi. *Modélisation d'écoulements compressibles avec transition de phase et prise en compte des états métastables*. PhD thesis, 2018.
- [14] Ghazi, H., James, F., and Mathis, H. Vapour-liquid phase transition and metastability. *ESAIM: ProcS*, 66:22–41, 2019.
- [15] J. W. Gibbs. *The Collected Works of J. Willard Gibbs, vol I: Thermodynamics*. Yale University Press, 1948.
- [16] P. Helluy, O. Hurisse, and E. Le Coupanec. Verification of a two-phase flow code based on an homogeneous model. *Int. J. Finite Vol.*, EDF Special Workshop:24, 2015.
- [17] P. Helluy and H. Mathis. Pressure laws and fast Legendre transform. *Math. Models Methods Appl. Sci.*, 21(4):745–775, 2011.
- [18] J.-B. Hiriart-Urruty and C. Lemaréchal. *Fundamentals of convex analysis*. Grundlehren Text Editions. Springer-Verlag, Berlin, 2001.
- [19] O. Hurisse. Application of an homogeneous model to simulate the heating of two-phase flows. *Int. J. Finite Vol.*, 11:37, 2014.
- [20] O. Hurisse. Numerical simulations of steady and unsteady two-phase flows using a homogeneous model. *Comput. & Fluids*, 152:88–103, 2017.
- [21] O. Hurisse and L. Quibel. A homogeneous model for compressible three-phase flows involving heat and mass transfer. *ESAIM: Proceedings and Surveys*, 2019.
- [22] F. James and H. Mathis. A relaxation model for liquid-vapor phase change with metastability. *Commun. Math. Sci.*, 14(8):2179–2214, 2016.
- [23] Lev Davidovich Landau and Evgenii M Lifshitz. *Statistical Physics: V. 5: Course of Theoretical Physics*. Pergamon press, 1969.
- [24] Robert G Mortimer. *Physical chemistry*. 3rd, 2008.
- [25] R. T. Rockafellar. *Convex analysis*. Princeton Landmarks in Mathematics. Princeton University Press, Princeton, NJ, 1997. Reprint of the 1970 original, Princeton Paperbacks.
- [26] R. Saurel, F. Petitpas, and R. Abgrall. Modelling phase transition in metastable liquids: application to cavitating and flashing flows. *J.Fluid Mech.*, 607:313–350, 2008.
- [27] E. F. Toro. *Riemann solvers and numerical methods for fluid dynamics*. Springer-Verlag, Berlin, third edition, 2009. A practical introduction.
- [28] A. Zein, M. Hantke, and G. Warnecke. Modeling phase transition for compressible two-phase flows applied to metastable liquids. *J. Comp. Phys.*, 229:1964–2998, 2010.

(Hala Ghazi) LABORATOIRE JEAN LERAY, UNIVERSITÉ DE NANTES & CNRS UMR 6629, BP 92208, F-44322 NANTES CEDEX 3, FRANCE

E-mail address: `hala.ghazi@univ-nantes.fr`

(François James) INSTITUT DENIS POISSON, UNIVERSITÉ D'ORLÉANS & CNRS UMR 7013, BP 6759, F-45067 ORLÉANS CEDEX 2, FRANCE

E-mail address: `francois.james@univ-orleans.fr`

(Hélène Mathis) LABORATOIRE JEAN LERAY, UNIVERSITÉ DE NANTES & CNRS UMR 6629, BP 92208, F-44322 NANTES CEDEX 3, FRANCE

E-mail address: `helene.mathis@univ-nantes.fr`